Chapter 4

Hopf dances near the tips of Busse balloons

4.1 Introduction

The (complex) Ginzburg-Landau equation exhibits bands of stable periodic patterns that are generically destabilized by the sideband (or Eckhaus, or Benjamin-Feir) instability mechanism. Moreover, the boundary of a Busse balloon near onset is generically given by a parabola – the Eckhaus parabola – of sideband destabilizations, see chapter 2. Ginzburg-Landau theory is a general and very powerful theory, however, it only applies to the asymptotically small part of a Busse balloon near onset.

Of course, one can in general not hope to obtain a full analytical control over an entire Busse balloon. As for the Ginzburg-Landau theory one should only expect to be able to capture small, but essential, parts of the Busse balloon by analytical means (see however Remark 1.1). Moreover, it is at present too ambitious to propose to develop a theory for 'far-from-equilibrium-patterns' that is as general as Ginzburg-Landau theory. Based on recent developments in the (mathematical) theory, we nevertheless claim it is possible to consider the above question in the setting of a well-specified class of problems: the stability and destabilization of nearly localized, spatially periodic patterns in reaction-diffusion equations, see Figure 4.1. This class of problems is especially interesting, since there are quite a number of results in the literature that indicate that these (singular) long wavelength periodic multi-pulse/front/spike patterns appear as the 'most stable' – i.e the last periodic patterns to destabilize – spatially periodic patterns [17, 44, 48, 49, 56, 58, 60, 68, 97]. This is also confirmed by the Busse balloon for the Gray-Scott system (1.1) presented in Figure 4.2(a): for decreasing A, stable patterns appear at a Ginzburg-Landau/Turing bifurcation and eventually disappear at a 'tip' at which the wavenumber k approaches zero (i.e. at which the wavelength of the patterns becomes large). Thus, these singular patterns may indeed represent an essential (but small) part of the Busse balloon. Complemen-

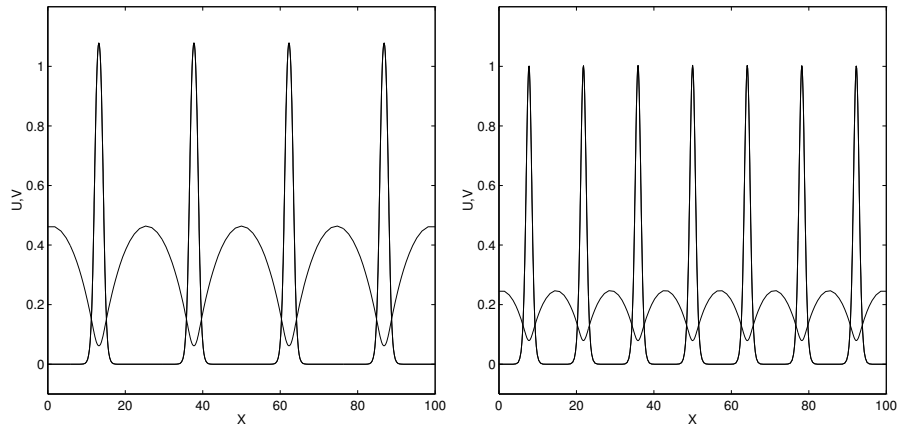

Figure 4.1: Two typical stationary, nearly localized, reversible spatially periodic patterns with different wavelengths L/wavenumbers k. These patterns coexist as stable solutions of the Gray-Scott model (1.1) with $A = \varepsilon^4 = 0.01$ and $B = 0.060$ [16].

tary to the small amplitude Ginzburg-Landau patterns that indicate the 'bottom' of the Busse balloon at which patterns appear, the nearly localized patterns may form the 'tip' of the Busse balloon at which the stable periodic patterns disappear.

Therefore, we focus in this chapter on the study of Busse balloons associated to periodic patterns in reaction-diffusion systems in one spatial dimension. In the numerical (first) part of the chapter, we do consider a 'full' Busse balloon, but only in the context of a very explicit, singularly perturbed two component model, the well-studied Gray-Scott equation,

$$\left\{ \begin{array}{rcrcrcl} U_t &=& U_{xx} &+& A(1-U) &-& UV^2 \\ V_t &=& \varepsilon^4 V_{xx} &-& BV &+& UV^2 \end{array} \right. , \tag{1.1}$$

in which $A, B > 0$ and $\varepsilon > 0$ are parameters (and $0 < \varepsilon \ll 1$ in the singularly perturbed setting). In the analytic part of this chapter, we restrict ourselves to the nearly-localized tip of the Busse balloon, in the context of a certain (sub)class of problems that a priori includes the patterns considered in the Gray-Scott model (see sections §4.1.2 and §4.3.5): the stability and destabilization of nearly localized reversible patterns in singularly perturbed two component reaction-diffusion equations.

The specific choice to restrict the analysis to singularly perturbed systems is motivated by the state-of-the-art of the mathematical theory for the existence and stability of nearly localized periodic patterns. There is a well-developed qualitative mathematical theory for (one-dimensional) localized structures, such as (homoclinic) pulses/spikes and (heteroclinic) fronts, in reaction-diffusion equations – see [76] and the references therein. By the methods developed in [35, 36, 78], it is possible to extend this theory

to nearly-localized spatially periodic patterns. However, at this point, the general theory does not provide the amount of quantitative information necessary to study the nearly homoclinic ($k = 0$) tip of Busse balloons in full detail. Such a more quantitative theory has been developed in the context of singularly perturbed reaction-diffusion equations, both for the localized patterns [17], as well as for the nearly-localized spatially periodic patterns [68]. We refer to section §4.6 for a discussion of the extension of our main results to non-singularly perturbed systems.

The generic mechanism proposed here – the *'Hopf dance near the tip of Busse balloons'* – is graphically presented in Figure 4.2. Figure 4.2(a) is the outcome of a comprehensive numerical study of the stability and existence boundaries in (parameter,wavenumber)-space of spatially periodic patterns of the Gray-Scott model, by means of continuation techniques (see especially [70]). Although the Gray-Scott system is one of the most thoroughly studied reaction-diffusion systems in the recent literature, see e.g. [16, 18, 23, 48, 49, 56, 57, 58, 62, 63, 66, 67, 73, 98], we are not aware of a comparable comprehensive (numerical) study of periodic patterns in the Gray-Scott model (a rough approximation of this Busse balloon, obtained by direct simulation the Gray-Scott model, has been presented in [56]; in [89] the same continuation approach has been used to study the stability of periodic patterns in lambda-omega systems, where it can be reduced to the much more simple case of constant coefficients). The *'Hopf dance'* is performed by two intertwined snaking curves of Hopf instabilities, denoted by $\mathcal{H}_{\pm 1}$ in Figure 4.2, that terminate in the limit $k = 0$ at the Hopf bifurcation of the limiting homoclinic pulse. Figure 4.2(b) gives a schematic sketch of the Hopf dance destabilization mechanism. The curve $\mathcal{H}_{+1}$, represents a Hopf destabilization in which all extrema of the pattern start to oscillate exactly in phase at the bifurcation; at $\mathcal{H}_{-1}$ the maxima (or minima) of the patterns that are one period away from each other begin to oscillate exactly out of phase. The Hopf dance gives the boundary of the Busse balloon a fine structure of alternating pieces of the curves $\mathcal{H}_{+1}$ and $\mathcal{H}_{-1}$, representing different types of destabilizations, separated by an infinite sequence of corners, or co-dimension 2 points.

The $\mathcal{H}_{\pm 1}$ Hopf instabilities stem from the intersections with the imaginary axis of the endpoints of a bounded curve of the spectrum associated to the linearized stability of the periodic pattern (see section §4.2). To leading order, this spectral curve is a straight line segment that, as a function of decreasing wavenumber k, rotates around its center while shrinking exponentially in length. At second order, the spectral curve is bent, and it is striking to note that its overall curvature oscillates with twice the frequency of the rotation, so that the most unstable point of the spectral curve cannot be an interior point, but must always be one of the two $\mathcal{H}_{\pm 1}$ endpoints. In this chapter, we refer to this oscillation as the *'belly dance'*.

A priori, the Hopf (and belly) dance performed by the (spectrum associated to the) periodic patterns in the Gray-Scott model may seem very special, and thus non-generic, behavior. However, this is not the case. In the second part of this chapter, §4.4–§4.5, we prove that both the Hopf and the belly dances occur in a class of two component, singularly perturbed reaction-diffusion systems that includes the gener-

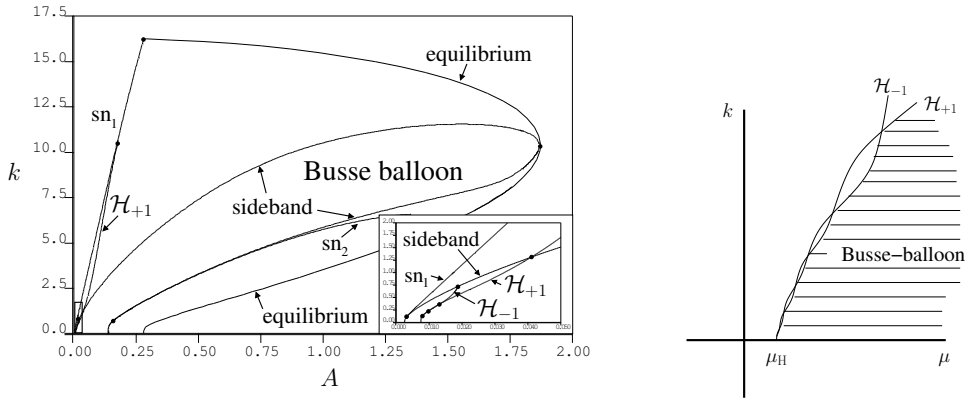

Figure 4.2: (a) A Busse balloon associated to the Gray-Scott equation, (1.1) with $B = 0.26$ and $\varepsilon^4 = 0.001$, embedded in the associated existence balloon, i.e. the region in (parameter, wavenumber)-space in which spatially periodic patterns exist (but are not necessarily stable). For decreasing A, the Busse balloon is initiated by a Turing/Ginzburg-Landau bifurcation; it ends at a 'homoclinic tip' at A of the order of ε^4. The boundary segments are labeled according to their type: for existence these are curves of folds (sn_1, sn_2) and of vanishing amplitude at equilibria; for stability these are curves of Hopf instabilities, sideband instabilities and also folds – the exact meaning and interpretation of these labels are discussed in detail in section §4.3. Bullets mark corners (co-dimension 2 points). The inset enlarges the rectangular region near the homoclinic ($k = 0$) limit at which the Hopf dance of the curves $\mathcal{H}_{\pm 1}$ occurs. Note that only the first three intersections of the curves $\mathcal{H}_{\pm 1}$ have been plotted. (b) A schematic sketch of the Hopf dance at the homoclinic tip of a Busse balloon; μ is a parameter and μ_{H} indicates the Hopf bifurcation value associated to the homoclinic pulse pattern that appears as $k \downarrow 0$.

alized Gierer-Meinhardt model [17]. Based on the Evans function analysis of [68], we give explicit formulas for the leading and next order geometry of the spectral curves associated to the stability of the nearly localized spatially periodic patterns in this class of systems. In particular, our formulas give explicit expressions (in terms of exponentially small quantities in ε) for the local (fine) structure of the boundary of the Busse balloon. Moreover, we identify the quantity that determines whether the limiting homoclinic $k = 0$ pulse is the last periodic pattern to become unstable as the parameter varies (called Ni's conjecture [60], see Remark 5.4). Similarly, we identify the quantity that determines the orientation of the belly dance, that is, whether the $\mathcal{H}_{\pm 1}$ endpoints of the spectral curves are always the most unstable or not. In the latter case, the actual stability boundary will be a smoothed out version of that obtained from considering the endpoints alone, see Figure 4.10 and section §4.6.

We conclude this chapter by a discussion of the robustness of the Hopf dance destabilization mechanism within larger classes of systems (section §4.6).

Remark 1.1 An important class of equations with a rich, and relatively easy to study, class of periodic patterns (or wave trains) is the widely studied complex Ginzburg-Landau equation. In the most simple case, the real Ginzburg-Landau equation, the boundary of the Busse balloon is in its entirety given by the (unbounded) Eckhaus parabola of sideband instabilities. For the general (complex) cubic Ginzburg-Landau equation, the Busse balloon may be non-existent, or its boundary may consist of certain Hopf bifurcations [54]. The structure of the Busse balloon becomes less simple, and for instance includes co-dimension 2 corners, for (extended) cubic-quintic Ginzburg-Landau equations that occur near the transition of super- to subcritical bifurcations [14, 30, 83, 84]. In fact, the analysis in [30] indicates that there may even be bounded Busse balloons in this case.

Remark 1.2 Some aspects of the Hopf dance destabilization mechanism were already found analytically in [68] for the special case of the classical Gierer-Meinhardt model. However, it was not yet recognized in [68] as a generic phenomenon, and not analyzed in detail.

4.1.1 The setting

In their most general form, two component reaction-diffusion equations in one spatial dimension are given by,

$$\left\{ \begin{array}{rcrcl} U_t & = & U_{xx} & + & F(U,V;\vec{\mu}) \\ V_t & = & D^2 V_{xx} & + & G(U,V;\vec{\mu}) \end{array} \right. \tag{1.2}$$

The reaction is described by the vector fields $F, G : \mathbb{R}^2 \to \mathbb{R}^2$ that depend on the parameter(s) $\vec{\mu} \in \mathbb{R}^m$ ($m \geq 1$) in the problem. The system is considered on the unbounded real line, i.e. $x \in \mathbb{R}$, and x is scaled such that the diffusion coefficient associated to U is 1; V diffuses with coefficient $D^2 > 0$.

The stationary problem associated to (1.2) consists of two purely second order ordinary differential equations in the time-like space variable x. Such equations always possess a reversible symmetry induced by spatial reflection $x \to -x$. Solutions that are reflection symmetric in x are called *reversible*, which is the case for all solutions that are relevant for our purposes. Reflection symmetric periodic patterns, or standing wave trains, of (1.1) are reversible periodic orbits and typically persist as periodic orbits under perturbation with an adjusted period L (or wavenumber k), e.g., [25, 71]. Hence, we can expect open regions of existence in the $(\vec{\mu}, k)$-parameter space.

Let $(U_{\mathrm{p}}(x;k), V_{\mathrm{p}}(x;k))$ be such a family of stationary spatially periodic patterns with associated periodic solutions $\gamma_{\mathrm{p}}(x;k)$ of the 4-dimensional (spatial) dynamical system for stationary solutions of (1.2). Existence regions then come as (maximal) connected regions $I_{\mathrm{e}}(\vec{\mu}) \subset \mathbb{R}$ in k for which $(U_{\mathrm{p}}(x;k), V_{\mathrm{p}}(x;k))$ exist. Note that for a given $\vec{\mu}$,

$I_{\mathrm{e}}(\vec{\mu})$ may only be one of several disjoint existence regions. The physically most relevant patterns are the solutions of (1.2) that are dynamically stable. In this chapter we are only concerned with spectral stability. We define $\sigma = \sigma(U_{\mathrm{p}}, V_{\mathrm{p}})$ as the spectrum associated to the linearization about a pattern $(U_{\mathrm{p}}(x;k), V_{\mathrm{p}}(x;k))$ (1.2) and call a pattern spectrally *stable* if $\sigma \cap \{\mathrm{Re}(\lambda) \geq 0\} = \{0\}$, and if the curve of σ through the origin has quadratic tangency, see e.g, [71]. Stable periodic patterns form a subset of $I_{\mathrm{e}}(\vec{\mu})$. Let $I_{\mathrm{s}}(\vec{\mu}) \subset I_{\mathrm{e}}(\vec{\mu})$ be a connected component of this subset in the sense that $(U_{\mathrm{p}}(x;k), V_{\mathrm{p}}(x;k))$ destabilizes as k approaches the boundary of $I_{\mathrm{s}}(\vec{\mu})$. A Busse balloon B_B of (1.2) is defined as a connected component of the $(\vec{\mu}, k)$-parameters of stable periodic patterns, that is,

$$B_B = \bigcup_{\vec{\mu} \in \mathbb{R}^m} (\vec{\mu}, I_s(\vec{\mu})) \subset \mathbb{R}^{m+1}, \tag{1.3}$$

see also Remark 1.3. For practical reasons, one often fixes $(m-1)$-components of $\vec{\mu}$ and only plots a two-dimensional cross-section of B_B in (μ_j, k)-space – see Figure 4.2.

The reversible symmetry has consequences for the (stability) boundary of the Busse balloon. According to [71], the following types of instabilities can generically occur along curves of the boundary. Where noted, this is with respect to a destabilizing mode $\mathrm{e}^{\mathrm{i}(\alpha t - \eta x)}$ (and its complex conjugate).

'Sideband'	curvature of the curve of σ at the origin changes sign through the instability (also called Benjamin-Feir or Eckhaus instability)
'Hopf'	$\alpha \neq 0$, $\eta \neq 0$ (also called Turing-Hopf)
'Turing'	$\alpha = 0$, $\eta \neq 0$
'Period doubling'	as Turing, but with $\eta = k/2$,
'Pure Hopf'	as Hopf but with $\eta = 0$,
'Fold'	the pattern undergoes a saddle-node bifurcation.

In all cases $\sigma \cap \{\mathrm{Re}(\lambda) \geq 0\} = \{0, \mathrm{i}\alpha, -\mathrm{i}\alpha\}$, where $\alpha = 0$ for sideband, fold and Turing.

Inspired by the Hopf dance observed in the Gray-Scott model, we focus in the analytic part of this chapter on the 'normal form model' for large amplitude pulse patterns to singularly perturbed equations given by

$$\left\{ \begin{array}{rcrcrcl} \varepsilon^2 U_t & = & U_{xx} & - & \varepsilon^2 \mu U & + & U^{\alpha_1} V^{\beta_1} \\ V_t & = & \varepsilon^2 V_{xx} & - & V & + & U^{\alpha_2} V^{\beta_2}, \end{array} \right. \tag{1.4}$$

in which $0 < \varepsilon \ll 1$. This model is known as the generalized Gierer-Meinhardt equation [17, 43, 44, 60, 97, 99]; $U(x,t), V(x,t)$ are scaled versions of their counterparts in (1.2) and are by construction $\mathcal{O}(1)$ w.r.t. ε. This equation was originally derived as leading order normal form model for large amplitude pulse patterns to singularly perturbed two component reaction-diffusion equations in [17]. It is derived from equations of the type (1.2) by imposing a couple of assumptions:

(A-i) the system has a stable 'background state' $(U(x,t),V(x,t)) \equiv (0,0)$;
(A-ii) the equations decouple at the linear level (i.e. as $\|(U,V)\|$ becomes small);
(A-iii) the nonlinearities grow algebraically and are 'separable' in a sense explained in §4.1.2.

We refer to section §4.1.2 for a sketch the derivation of (1.4) and the conditions on its parameters. As for the Gray-Scott model, there are many indications in the literature that tip of the Busse balloon associated to (1.4), i.e. the last region in which stable periodic patterns exist, is also formed by nearly homoclinic, nearly localized, spatially periodic patterns [17, 44, 60, 68, 97]. More specifically, the limiting homoclinic $k = 0$ pattern generally appears as 'the last pattern to become unstable' – see §4.5 and particularly Remark 5.4 on Ni's conjecture. In section §4.4, (part of) the existing literature on the existence and stability of stationary singular spatially periodic patterns to (1.4) is summarized.

Remark 1.3 Reaction-diffusion equations naturally also exhibit traveling spatially periodic patterns, or wave trains, i.e. non-stationary solutions that are periodic in space and in time. For these patterns, one can also define the concept of a Busse balloon (in a completely equivalent fashion). However, in this chapter we only consider stationary periodic patterns.

4.1.2 The normal form model

In this section we give a brief derivation of (1.4) as normal form model for large amplitude pulses in the general class of singularly perturbed (two component) reaction-diffusion models (1.2). First, we bring the equation into a singularly perturbed form that satisfies the first two assumptions (*(A-i)* and *(A-ii)*,

$$\left\{ \begin{array}{rclcrcl} U_t & = & U_{xx} & - & \mu U & + & H_1(U,V;\varepsilon,\vec{\mu}) \\ V_t & = & \varepsilon^4 V_{xx} & - & V & + & H_2(U,V;\varepsilon,\vec{\mu}), \end{array} \right. \tag{1.5}$$

where $H_1(U,0) = H_2(U,0) \equiv 0$. Note that the parameter μ controls the (relative) decay rates of U and V (i.e. $\mu > 0$). Singular equations of this type generally exhibit localized patterns that are singular in various ways: *(E-i)* the 'fast' V-components are spatially localized in regions in which the 'slow' component U remains at leading order constant; *(E-ii)* the U-components vary slowly in regions in which V is exponentially small; *(E-iii)* the amplitude of both U- and V-components scale with a negative power of ε – i.e. they are asymptotically large. Therefore, it is natural to scale out the asymptotic magnitudes of U and V,

$$\tilde{U}(x,t) = \varepsilon^r U(x,t), r \geq 0,\ \tilde{V}(x,t) = \varepsilon^s V(x,t), s \geq 0,$$

so that $\tilde{U}(x,t)$ and $\tilde{V}(x,t)$ are $\mathcal{O}(1)$ w.r.t. ε; the magnitudes r and s are a priori unknown. The following assumption on the asymptotic behavior of the nonlinearities $H_{1,2}(U,V)$, which is the technical version of assumption *(A-iii)*, is crucial to the derivation of (1.4),

$$H_i(U,V) = H_i(\frac{\tilde{U}}{\varepsilon^r},\frac{\tilde{V}}{\varepsilon^s}) = \tilde{U}^{\alpha_i}\tilde{V}^{\beta_i}\varepsilon^{-(r\alpha_i+s\beta_i)}\left[h_i + \hat{\varepsilon}\tilde{H}(\tilde{U},\tilde{V};\varepsilon)\right], \tag{1.6}$$

in which $\hat{\varepsilon}$ is some positive power of ε and $\tilde{H}_i = \mathcal{O}(1)$ w.r.t. ε. Hence, it is assumed that the growth of nonlinear terms $H_i(U,V)$ for U,V large is dominated by the algebraic expression $U^{\alpha_i}V^{\beta_i}$. Note that this part of assumption *(A-iii)* is quite natural, as are assumptions *(A-i)* and *(A-ii)* – see Remark 1.4. However, there is an additional part to assumption *(A-iii)* that is more restrictive: the asymptotic decomposition (1.6) is also assumed to be separable, in the sense that the leading order terms (for U,V large) can be factored out of $H_i(U,V)$. Note that this assumption implies that the leading order behavior for large solutions also dominates as these solutions are no longer large. See §4.6 and Remark 1.4 for a discussion of this issue and its relation to the (conjectured) generiticity of the Hopf dance. The magnitudes r and s of U and V can now be determined in terms of $\alpha_1, \alpha_2, \beta_1, \beta_2$ by the assumption that (large, singular) pulse type patterns can indeed exist as solutions of (1.5),

$$r = \frac{\beta_2 - 1}{d} > 0,\ s = -\frac{\alpha_2}{d} > 0,\ \text{ with } d \stackrel{\text{def}}{=} (\alpha_1 - 1)(\beta_2 - 1) - \alpha_2\beta_1 > 0, \tag{1.7}$$

see [17]. This analysis also yields that $h_j > 0$, for $j = 1, 2$, and that the parameter(s) $\vec{\mu} = (\mu, \alpha_1, \alpha_2, \beta_1, \beta_2)$ in (1.4) must satisfy the following conditions,

$$\mu > 0,\ d > 0,\ \alpha_2 < 0,\ \beta_1 > 1,\ \beta_2 > 1. \tag{1.8}$$

By introducing the spatial scale $\tilde{x} = x/\varepsilon$ and neglecting all tildes, equation (1.5) can now at leading order be brought into the 'normal form' (1.4).

Remark 1.4 A more general model that satisfies *(A-i)* and *(A-ii)* and that generalizes *(A-iii)* to non-separable nonlinearities is,

$$\left\{ \begin{array}{rcrcrcl} \varepsilon^2 U_t & = & U_{xx} & - & \varepsilon^2[\mu U - F_1(U;\varepsilon)] & + & F_2(U,V;\varepsilon), \\ V_t & = & \varepsilon^2 V_{xx} & - & V & + & G(U,V;\varepsilon). \end{array} \right. \tag{1.9}$$

Note that especially the fact that there is a spatial nonlinearity $F_1(U;\varepsilon) \neq 0$ distinguishes this model from the Gray-Scott/Gierer-Meinhardt types models in the literature [13]. We will come back to this generalized model in the discussion of the (non-)generic effect of the 'belly dance' in section §4.6.

4.2 Preliminaries I: The stability of periodic patterns

In this section, we sketch several aspects of the literature on the stability of periodic patterns in reaction-diffusion equations. The presentation is largely based on [35, 36, 68, 70, 71, 78]. For simplicity, we restrict ourselves to the two components setting of (1.2). However, the ideas presented here can be readily extended to N-component systems. Moreover, (1.2) includes all other, more specific, models considered in this chapter.

4.2.1 The structure of the spectrum

The spectral stability problem associated to a stationary, spatially periodic solution $(U_{\rm p}(x;k), V_{\rm p}(x;k))$ of (1.2) with respect to perturbations (for instance) in $BC_{\rm unif}(\mathbb{R}, \mathbb{R}^2)$, i.e. the space of bounded and uniformly continuous functions, is obtained by substitution of

$$U(x,t) = U_{\rm p}(x;k) + u(x)e^{\lambda t}, \;\; V(x,t) = V_{\rm p}(x;k) + v(x)e^{\lambda t},$$

into (1.4), followed by linearization. This yields the system,

$$\left\{ \begin{array}{rcl} \lambda u &=& u_{xx} + \partial_U F(U_{\rm p}(x), V_{\rm p}(x))u + \partial_V F(U_{\rm p}(x), V_{\rm p}(x))v \\ \lambda v &=& D^2 v_{xx} + \partial_U G(U_{\rm p}(x), V_{\rm p}(x))u + \partial_V G(U_{\rm p}(x), V_{\rm p}(x))v \end{array} \right. \tag{2.1}$$

Since $x \in \mathbb{R}$, (2.1) can be written in the form of a 4-dimensional (linear) system,

$$\dot{\phi}(\xi) = \mathcal{A}_{\rm p}(\xi; \lambda, L, \varepsilon)\phi(\xi), \tag{2.2}$$

where $\phi = (u, p = Du_\xi, v, q = v_\xi)^t$ in the scaled spatial variable $\xi = x/D$ and the dot denotes differentiation with respect to ξ. Note that ξ is introduced in anticipation of the singularly perturbed setting in which ξ represents the 'fast' spatial scale. For the same reason, we introduce L as half of the wavelength of the periodic pattern $(U_{\rm p}, V_{\rm p})$, i.e., with a slight abuse of notation, $(U_{\rm p}(x;k), V_{\rm p}(x;k)) = (U_{\rm p}(\xi;L), V_{\rm p}(\xi;L))$ with $L = \pi/kD$. Therefore, the periodic matrix $\mathcal{A}_{\rm p}(\xi;\lambda,k)$ in (2.2) is given by,

$$\mathcal{A}_{\rm p}(\xi;\lambda,L) = \begin{pmatrix} 0 & D & 0 & 0 \\ D(\lambda - \partial_U F(U_{\rm p}(\xi;L), V_{\rm p}(\xi;L))) & 0 & -D\partial_V F(U_{\rm p}(\xi;L), V_{\rm p}(\xi;L)) & 0 \\ 0 & 0 & 0 & 1 \\ -\partial_U G(U_{\rm p}(\xi;L), V_{\rm p}(\xi;L)) & 0 & (\lambda - \partial_V G(U_{\rm p}(\xi;L), V_{\rm p}(\xi;L))) & 0 \end{pmatrix}. \tag{2.3}$$

Since $\mathcal{A}_{\rm p}(\xi;\lambda,L)$ is $2L$ periodic, solutions to (2.2) can (by Floquet theory) be assumed to be of the form

$$\phi(\xi) = \psi(\xi)e^{c\xi} \;\text{ for some }\; c \in \mathbb{C} \;\text{ and }\; \psi(\xi) \;\; 2L-\text{periodic}.$$

However, the perturbations $\phi(\xi;\lambda)$ must be in $BC(\mathbb{R}, \mathbb{C}^4)$, so that $c = i\tilde{c} \in i\mathbb{R}$. Hence,

$$\phi(\xi + 2L; \lambda) = \gamma\, \phi(\xi;\lambda) \;\text{ for a }\; \gamma \in \mathbb{S}^1, \tag{2.4}$$

since $\gamma = e^{2i\tilde{c}L} \in \mathbb{C}$ with $|\gamma| = 1$. Note that if $\phi(\xi;\lambda)$ satisfies condition (2.4) in one particular point ξ, it satisfies (2.4) everywhere. Since bounded solutions of (2.2) can be decomposed into a combination of functions $\phi(\xi;\lambda)$ that satisfy (2.4) for some $\gamma \in \mathbb{S}^1$, it follows that the spectrum $\sigma((U_{\rm p}, V_{\rm p}))$ of the stability problem associated to the periodic pattern $(U_{\rm p}(\xi;L), V_{\rm p}(\xi;L))$ entirely consists of γ-eigenvalues [35], i.e. $\lambda(\gamma) \in \mathbb{C}$ such that there is a solution $\phi(\xi)$ of (2.2) that satisfies (2.4) for some $\gamma \in \mathbb{S}^1$. Thus, by varying γ over $\mathbb{S}^1$, we may conclude that $\sigma((U_{\rm p}, V_{\rm p}))$ is the union of – a priori countably many – bounded curves $\Lambda(L;\vec{\mu})$ with

$$\Lambda(L;\vec{\mu}) = \{\lambda \in \mathbb{C} : \lambda(\gamma) \;\text{ is a }\; \gamma-\text{eigenvalue}, \gamma \in \mathbb{S}^1\} \tag{2.5}$$

(see [35, 70, 78]). In general, these curves can either be a smooth image of $\mathbb{S}^1$ or have a more degenerate structure. In particular, they often form closed loops that are isolated connected components of the spectrum.

4.2.2 Reversibility: the collapse of $\Lambda(L;\vec{\mu})$

Due to the reversibility symmetry in both the equation (1.2) and the patterns $(U_{\rm p}(\xi;L),V_{\rm p}(\xi;L))$, the spectral loops $\Lambda(L;\vec{\mu})$ (2.5) collapse to branches with well-defined endpoints $\partial_{\pm}\Lambda(L;\vec{\mu})$. To see this, we need to be more explicit about nature of these symmetries. First, we may define $\xi=0$ as a reflection point for the pattern $(U_{\rm p}(\xi;L),V_{\rm p}(\xi;L))$, i.e. we may assume that $(U_{\rm p}(-\xi;L),V_{\rm p}(-\xi;L))=(U_{\rm p}(\xi;L),V_{\rm p}(\xi;L))$ for all ξ. Note that,

$$(U_{\rm p}(L+\xi),V_{\rm p}(L+\xi;L))=(U_{\rm p}(\xi-L),V_{\rm p}(\xi-L))=(U_{\rm p}(L-\xi),V_{\rm p}(L-\xi))$$

by the $2L$-periodicity of $(U_{\rm p}(\xi;L),V_{\rm p}(\xi;L))$. Hence, $(U_{\rm p}(\xi;L),V_{\rm p}(\xi;L))$, and thus $\mathcal{A}_{\rm p}(\xi;L)$ (2.3), is reflection symmetric with respect to all points $\xi=kL$, $k\in\mathbb{Z}$. Thus, system (2.2) is also reversible, that is, if $\phi(\xi)$ is a solution, then so is,

$$\hat{\phi}(\xi)=R\phi(-\xi)=(u(-\xi),-p(-\xi),v(-\xi),-q(-\xi))$$

(with involution $R:\mathbb{R}^4\to\mathbb{R}^4$). Now, if λ is a γ-eigenvalue, and $\phi(\xi)$ its associated γ-eigenfunction, then (by (2.4)),

$$\hat{\phi}(\xi+2L)=R\phi(-\xi-2L)=\frac{1}{\gamma}R\phi(-\xi)=\overline{\gamma}\hat{\phi}(\xi),$$

since $\gamma\in\mathbb{S}^1$. In other words, $\hat{\phi}(\xi)$ is a $\overline{\gamma}$-eigenfunction (2.4), which implies that λ is both a γ- and a $\overline{\gamma}$-eigenvalue. Hence, as γ is varied over $\mathbb{S}^1$, every point $\lambda(\gamma)\in\Lambda(L;\vec{\mu})$ is visited twice, except for the points $\lambda(\pm1)$ since $\gamma=\overline{\gamma}$ for $\gamma=\pm1$: the loop $\Lambda(L;\vec{\mu})$ collapses to a branch with endpoints $\partial_{\pm}\Lambda(L;\vec{\mu})=\lambda(\pm1)$

If a branch $\Lambda(L;\vec{\mu})$ crosses through the imaginary axis as a function of $\vec{\mu}$, it is very likely that one of the endpoints $\partial_{\pm}\Lambda(L;\vec{\mu})$ is the first point of $\Lambda(L;\vec{\mu})$ to make contact with the imaginary axis. Indeed, if this occurs, it is robust under perturbations. However, note that this is not necessary: $\Lambda(L;\vec{\mu})\subset\mathbb{C}$ is in general curved, so $\Lambda(L;\vec{\mu})$ may be tangent to the imaginary axis at its point $\lambda(\gamma)$ of first contact, i.e. $\lambda(\gamma)$ may certainly be an interior point with $\gamma\neq\pm1$. Even when $\Lambda(L;\vec{\mu})\subset\mathbb{R}$, the possibility that $\Lambda(L;\vec{\mu})$ is folded cannot be excluded, so that the first point of contact of $\Lambda(L;\vec{\mu})$ with the imaginary axis is not necessarily an endpoint $\partial_{\pm}\Lambda(L;\vec{\mu})$, but possibly an interior point at the fold. Nevertheless, it can be expected that the ±1-eigenvalues do play a dominant role in the stability and bifurcation analysis of reversible periodic patterns $(U_{\rm p}(\xi;L),V_{\rm p}(\xi;L))$. And thus, the bifurcations associated to these eigenvalues can be expected to turn up abundantly in the study of Busse balloons B_B.

We therefore define $\mu_{\pm}$ as the following critical value of μ, where μ represents one of the m components of $\vec{\mu}$: ${\rm Re}[\sigma(U_{\rm p},V_{\rm p})]<0$ for $\mu<\mu_{\pm}$, ${\rm Re}[\sigma(U_{\rm p},V_{\rm p})]=0$ only for a $\partial_{\pm}\Lambda(L;\vec{\mu})\in\sigma(U_{\rm p},V_{\rm p})$ at $\mu=\mu_{\pm}$ and ${\rm Re}[\partial_{\pm}\Lambda(L;\vec{\mu})>0$ for $\mu>\mu_{\pm}$ (this situation occurs in the Gray-Scott system, §4.3, and in the normal form model (1.4), §4.5). A priori, we need to distinguish between two cases: ${\rm Im}[\partial_{\pm}\Lambda(L;\mu=\mu_{\pm})]=0$ and ${\rm Im}[\partial_{\pm}\Lambda(L;\mu=\mu_{\pm})]\neq0$. However, in this chapter we focus on the latter case. We

refer to [68] for an example at which $\partial_-\Lambda(L;\mu_j=\mu_\pm)\in\mathbb{R}$ initiates a saddle node bifurcation.

The $+1$-eigenfunction $\phi(\xi;\lambda(+1))$ associated to $\partial_+\Lambda(L;\mu=\mu_+)$ is $2L$-periodic (by (2.4)). Since $\partial_+\Lambda(L;\mu=\mu_+)$ induces a Hopf instability if $\mathrm{Im}[\partial_+\Lambda(L;\mu=\mu_+)]\neq 0$ [71], this means that the destabilization at $\mu=\mu_+$ initiates an oscillation at which all extrema of the pattern $(U_{\mathrm{p}}(\xi;L),V_{\mathrm{p}}(\xi;L))$ move in phase. Note that description is only based on linear data, without further analysis it is not possible to extract information about the nonlinear, long-time, behavior beyond the bifurcation. Nevertheless, this linear prediction agrees with the (subcritical) Hopf bifurcation destabilization of $+1$-type most commonly encountered in simulations of the Gray-Scott and (classical) Gierer-Meinhardt equations, see [16, 43, 44, 48, 49, 56, 58, 68, 97].

If $\gamma=-1$, i.e. if $\partial_-\Lambda(L;\mu=\mu_-)\notin\mathbb{R}$ initiates the bifurcation, the linear dynamics are driven by a -1-eigenfunction $\phi(\xi;\lambda(-1))$ that is periodic with a doubled period $4L$,

$$\phi(\xi+4L;\lambda(-1))=-\phi(\xi+2L;\lambda(-1))=\phi(\xi;\lambda(-1))$$

(2.4). Thus, the Hopf instability driven by $\partial_-\Lambda(L;\mu=\mu_-)\notin\mathbb{R}$ induces an out of phase oscillation when the pattern $(U_{\mathrm{p}}(\xi;L),V_{\mathrm{p}}(\xi;L))$ destabilizes: the initial (linear) dynamics of (1.2) on an interval (ξ_0,ξ_0+2L) are opposite to those on the neighboring intervals (ξ_0-2L,ξ_0) and (ξ_0+2L,ξ_0+4L), and identical to the dynamics on the intervals that are at a distance of $4Lk$, $k\in\mathbb{Z}$. We are not aware of any simulations in the literature on Gray-Scott or Gierer-Meinhardt type models that exhibit this type of behavior near a Hopf bifurcation, see however sections §4.3 and §4.5.

In this chapter, we will denote the locus if instability induced by $\partial_\pm\Lambda(L;\mu=\mu_\pm)\notin\mathbb{R}$ by the manifolds $\mathcal{H}_{\pm1}\subset\partial B_B$ in the $(\vec{\mu},k)$-space.

4.2.3 An Evans function approach

It is well-known that the spectrum associated to spatially periodic patterns can be studied by an Evans function [32, 35, 36, 64, 68]. Here we sketch the construction of such an Evans function based on [35, 36]. First, we consider a fundamental (matrix) solution $\Phi(\xi;\lambda)$ of (2.2) and define its associated monodromy matrix $\mathcal{M}_L(\lambda)$ by

$$\Phi(\xi+2L;\lambda)=\Phi(\xi;\lambda)\mathcal{M}_L(\lambda). \tag{2.6}$$

Note that the existence of the (constant coefficients) matrix $\mathcal{M}_L(\lambda)$ follows from the fact $\mathcal{A}_{\mathrm{p}}(\xi;\lambda,L)$ is $2L$-periodic (2.3), so that $\Phi(\xi+2L;\lambda)$ also is a fundamental matrix solution of (2.2). Now, let $\vec{v}\in\mathbb{C}^4$ be an eigenvector of $\mathcal{M}_L(\lambda)$ with eigenvalue $\rho\in\mathbb{C}$, and define the solution $\phi(\xi)$ of (2.2) by $\phi(\xi;\lambda)=\Phi(\xi;\lambda)\vec{v}$, then

$$\phi(\xi+2L)=\Phi(\xi+2L)\vec{v}=\Phi(\xi)\mathcal{M}_L\vec{v}=\Phi(\xi)\rho\vec{v}=\rho\Phi(\xi)\vec{v}=\rho\phi(\xi).$$

Thus, $\phi(\xi)$ is a ρ-eigenfunction (2.4), and it follows that λ is a γ-eigenvalue if and only if $\mathcal{M}_L(\lambda)$ has an eigenvalue $\rho=\gamma\in\mathbb{S}^1$. Therefore, we define the Evans function

$\mathcal{D}(\lambda, \gamma; L)$ associated to the stability problem (2.2) by

$$\mathcal{D}(\lambda, \gamma; L) = \det\left[\mathcal{M}_L(\lambda) - \gamma \,\mathrm{Id}\right],\ \lambda \in \mathbb{C}, \gamma \in \mathbb{S}^1. \tag{2.7}$$

Hence, $\lambda(\gamma)$-eigenvalues correspond to zeroes of $\mathcal{D}(\lambda, \gamma)$. It is straightforward to check that these zeroes do not depend on the choice of the fundamental matrix solution $\Phi(\xi; \lambda)$. Nevertheless, the precise choice of $\Phi(\xi; \lambda)$ can be crucial: in the case of singularly perturbed systems, it is possible to construct a $\Phi(\xi; \lambda)$ so that the zeroes of $\mathcal{D}(\lambda, \gamma; L)$ can be determined analytically – see [32, 68] and §4.4.2.

4.3 A Busse balloon for the Gray-Scott model

In this section we discuss details of the (construction of the) Busse balloon, and the larger existences balloon, for the Gray-Scott model (1.1) as presented in Figure 4.2(a). The Busse balloon consists of stationary spatially periodic solutions of the 4-dimensional (spatial) dynamical system associated to (1.1). These spatial patterns correspond to periodic solutions of this 4-dimensional system with period, or wavelength, L ($k = 2\pi/L$ with $k =$ the wavenumber of the patterns). In all numerical computations we used the software AUTO [10] and fixed B at 0.26, ε^4 at 0.001, which means $\varepsilon \approx 0.18$, and varied A and L or equivalently k. In §4.3.5 we will bring equation (1.1) into a form that's comparable to the normal form model (1.4) and discuss the similarities/differences between the models.

4.3.1 Existence region

Before describing the Busse balloon, we discuss several aspects of the existence region in which the Busse balloon is embedded. As a consequence of the reversible symmetry discussed in §4.2.2, the 4-dimensional ODE reduction of (1.1) is also reversible and we can thus apply the 'reversible Lyapunov center theorem' [9]. This theorem guarantees the existence of reversible periodic orbits, or: spatially periodic patterns, in the vicinity of an equilibrium, i.e. of a homogeneous background state $(U, V) \equiv (\bar{U}, \bar{V})$ of (1.1). To apply the theorem, we first define ν_j, $j = 1, ..., 4$, as the eigenvalues associated to the linearization around an equilibrium – note that this linearization corresponds to (2.1) with $\lambda = 0$ and $(U_\mathrm{p}, V_\mathrm{p}) \equiv (\bar{U}, \bar{V})$. By the symmetry, the set of eigenvalues ν_j is reflection symmetric about the real *and* imaginary axes – see Figure 4.3. The center theorem can be applied if $\nu_j = \mathrm{i}\eta$, $\eta > 0$, for some j – see Remark 3.1 – and if all such modes are non-resonant. It states that there exists, within the 4-dimensional phase space, a two-dimensional manifold containing the equilibrium which is fibered by periodic orbits whose wavenumbers converges to η as one approaches the equilibrium. Since $i\eta$ is a purely imaginary spatial eigenvalue, η corresponds to a wave number k, we therefore refer to η as a linear wavenumber.

By the Lyapunov center theorem, a natural starting point for finding symmetric stationary spatially patterns is an unstable (Remark 3.1) background state. The

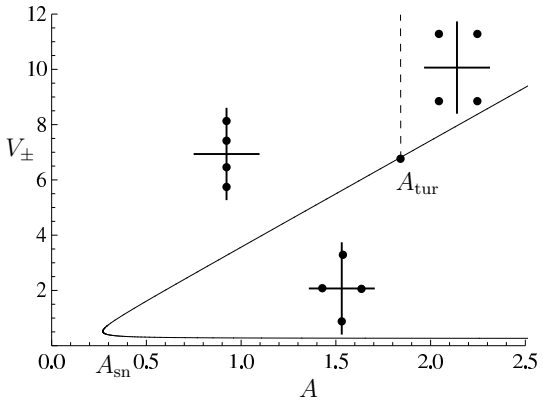

Figure 4.3: The branches $V_\pm$ as function of A of the background states $(U_\pm, V_\pm)$ of (1.1). The insets are sketches of the three qualitatively different distributions of the associated eigenvalues $\nu_j \in \mathbb{C}$, $j = 1, \ldots, 4$, one for the lower branch V_-, and two for the upper branch V_+ (one to the left and one to the right of the Turing instability).

background states of (1.1) are

$$U_0 = 1, V_0 = 0, \quad U_\pm = \frac{1}{2A}\left(A \mp \sqrt{A^2 - 4AB^2}\right), V_\pm = \frac{1}{2B}\left(A \pm \sqrt{A^2 - 4AB^2}\right),$$

where the conjugate pair $(U_\pm, V_\pm)$ undergoes a fold, or saddle node, bifurcation at $A_{\rm sn}$ determined by the condition $A = 4B^2$ (i.e. $A_{\rm sn} = 0.2704$ here). Thus, three real solutions exist for $A > A_{\rm sn}$. It can be checked that (U_0, U_0) is stable for all parameter values, that (U_-, U_-) is always unstable, and that (U_+, V_+) becomes stable through a Turing bifurcation for increasing A at $A_{\rm tur}$ (≈ 1.87 for the parameter values chosen here). We refer to [56] for more (analytical and computational) details on the Turing/Ginzburg-Landau bifurcation in the Gray-Scott model. Within the 4-dimensional ODE reduction, the Turing bifurcation corresponds to the $1:1$ reversible Hopf bifurcation, see Figure 4.3.

Thus, by the Lyapunov center theorem, and by Figure 4.3, two one-parameter families of small amplitude periodic patterns emerge near the equilibrium (U_+, V_+) for each $A \in (A_{\rm sn}, A_{\rm tur})$, one for each (non-resonant) pair of linear wavenumbers η. We denote the positive linear wavenumbers by $\eta_\pm(A)$ ordered so that $\eta_+ > \eta_-$. At the fold point $A = A_{\rm sn}$, we have $\eta_- = 0$ and the corresponding eigenvalue becomes real when continuing along the (U_-, V_-)-branch. At the Turing bifurcation, $\eta_- = \eta_+$, and the eigenvalues move off the imaginary axis when increasing A. A single one-parameter family emerges near (U_-, V_-), but these turn out to be of no interest to us.

In the (A, k)-parameter plane, the curves $\eta_\pm(A)$ provide part of the boundary of the existence region of periodic patterns. We denote these curves in Figure 4.2(a) by

'equilibrium'. The aforementioned two one-parameter families of periodic patterns bifurcate off $\eta_\pm(A)$, respectively, so that periodic patterns exist for $k < \eta_+$ and $k > \eta_-$. In fact, numerically we find that the two families are connected so that the patterns exist for $k \in (\eta_-, \eta_+)$ and $A \in (A_{\rm sn}, A_{\rm tur})$. Near the Turing bifurcation this is the well-known parabola shaped 'Ginzburg-Landau existence region' – see section §4.3.2 and [56].

At $A = A_{\rm sn}$ and $k = \eta_+(A_{\rm sn})$, the boundary has a corner and continues as a curve of folds, or saddle node bifurcations, of periodic orbits, denoted by '$\rm sn_1$'. While it is entirely expected that the fold of the underlying equilibrium induces a fold of the periodic solutions, we are not aware of any reference for a rigorous proof in the literature. The relevant existence boundary emerging from η_- when decreasing A from $A_{\rm tur}$ is slightly more involved. Between $A_{\rm tur}$ and $A \approx 1.3$, it involves period doubling bifurcations, but we omit details of this here as it lies outside the stability region (i.e. the Busse balloon). For smaller values of A, the relevant boundary is the fold curve '$\rm sn_2$'.

Remark 3.1 The assumption that $\nu_j(0) \in \mathrm{i}\mathbb{R}$ implies that $\lambda = 0$ lies in the spectrum associated to the background state $(\bar{U}, \bar{V})$ as solution of the PDE (1.2) – see section §4.2.1. Perturbing the real part of λ away from zero, typically implies that such purely imaginary solutions persist with an adjusted linear wavenumber. Conversely, we locally find a curve $\lambda(\eta)$ transversely crossing the imaginary axis. It thus follows that under the conditions of the Lyapunov center theorem, the underlying equilibrium is typically *unstable* as a solution of the PDE.

4.3.2 The Busse balloon

We continue the discussion of Figure 4.2(a), now looking at the stability boundaries, i.e. at the Busse balloon. Near the Turing instability we find the expected parabola shaped Eckhaus stability region bounded by sideband instabilities. Note that the existence and (side band) type of these boundaries has been proved rigorously near the Turing bifurcation by the Ginzburg-Landau analysis presented in [56]. Here, we extended these curves beyond the (asymptotically small) Ginzburg-Landau region, using the method described in [70]. A priori these sideband curves are only sufficient for establishes instability, since other instabilities could occur beyond the Ginzburg-Landau setting. However, we checked that this does not happen by finite difference approximations of the spectrum at regular intervals along the curves. In addition, there may in principle be an isolated region of unstable periodic patterns in the interior of the Busse balloon, but this is not the case, at least on the grid where we checked.

For decreasing values of k, the lower branch of sideband instabilities hugs very close to the fold curve '$\rm sn_2$', until it appears to merge with it. It should be noted that it is in this region in parameter space, and in particular for parameters that cross the curve '$\rm sn_2$' beyond the point where it has merged with the sideband curve, that the PDE dynamics exhibit the well-known and well-studied (but still largely not understood)

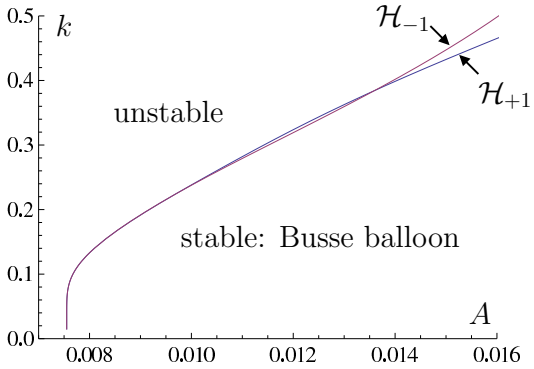

Figure 4.4: The $\mathcal{H}_{\pm}$ Hopf instabilities near the long wavelength limit of the Busse balloon; compare to Figure 4.2(a).

phenomenon of self-replicating pulses, see [23, 48, 57, 62, 66, 67, 73].

The upper branch of sideband instabilities similarly merges with the fold curve 'sn_1', however the sideband curve is no longer the stability boundary here. Instead, at $A \approx 0.041$, a curve $\mathcal{H}_{+1}$ of Hopf instabilities crosses the sideband curve – which generates a co-dimension 2 corner – and becomes the stability boundary. Following this curve for decreasing values of A we find another corner when a second curve, $\mathcal{H}_{-1}$, of Hopf instabilities crosses the first and takes over the stability boundary. These two curves repeatedly intersect and generate a sequence of corners in the stability boundary, see Figure 4.4. This is the generic Hopf dance destabilization mechanism that is the central theme of this manuscript. We discuss more details in the next subsection.

We continued the Hopf curves numerically up to $k = 0.01$ and observe a near vertical tangency, so that we predict the limiting value to be $A \approx 0.00755$. Since $\varepsilon \approx 0.18$ is not very small, this compares reasonably well to the predicted value for $\varepsilon \to 0$ of $A \approx 0.0049$ which we compute (analytically) from the results in [16, 18].

4.3.3 The Hopf dance and the rotation of the spectrum

The $\mathcal{H}_{\pm 1}$ curves can locally be seen as graphs of functions $A_{\pm}(k)$ over the k-axis (Figure 4.4). In Figure 4.5(a), we plot the difference $A_+(k) - A_-(k)$ over the first two crossings of $\mathcal{H}_{\pm 1}$. We plot this same difference for a larger interval of k values in Figure 4.5(b), where we have also blown up the difference by an ad hoc guess for an exponential decay factor (and where we have switched to $L = 2\pi/k$ for convenience). The result is a sinusoidal curve and we conjecture that this is the first part of an infinite 'Hopf dance' as L increases. Note that this sinusoidal shape and exponential decay of the parameter as function of the wavelength L is confirmed by the analysis of the normal form model in section §4.5.1 (see especially Corollary 5.5).

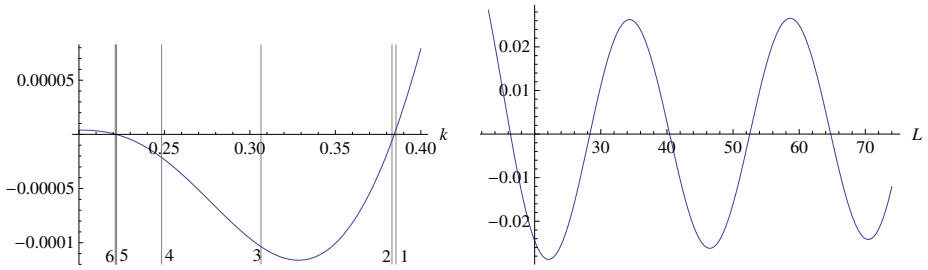

Figure 4.5: (a) The difference $A_+(k) - A_-(k)$ for k values including the first two crossing points of the curves $\mathcal{H}_{\pm 1}$. The vertical lines and their labels correspond to the k-values and the labels of the curves plotted in Figure 4.6. (b) The blown up difference $(A_+(L) - A_-(L))\exp(0.27L)$ over more intersections of $\mathcal{H}_\pm$.

Each point $(A_\pm(k), k)$ corresponds to a critical intersection of the spectrum $\sigma(U_\mathrm{p}, V_\mathrm{p})$ associated to a spatially periodic pattern $(U_\mathrm{p}, V_\mathrm{p})$ with the imaginary axis. As discussed in §4.2.1, this means that there are γ-eigenvalues $\lambda(\gamma_\pm) \in \mathrm{i}\mathbb{R}$ such that $\mathrm{Re}(\partial_\gamma \lambda(\gamma_\pm)) = 0$. It turns out that both spectral curves stem from the continuation of the same curve $\Lambda(L)$ and that this is the spectral curve, denoted by $\Lambda_\mathrm{h}(L)$, that shrinks to the (discrete) eigenvalue $\lambda_h \in \mathbb{C}$ associated to the homoclinic pulse that appears in the limit $L \to \infty$ (or $k \downarrow 0$); $\Lambda_\mathrm{h}(L)$ is – by definition – parametrized by $\lambda_\mathrm{Ho}(\gamma; A, k \text{ or } L)$ (see (2.5)). Moreover, we find that $\gamma_+ \equiv +1$ and $\gamma_- \equiv -1$ for all k, which at least locally is not surprising, since $\gamma = +1$ and $\gamma = -1$ represent the endpoints of the bounded curve $\Lambda_\mathrm{h}(L)$ (section §4.2.2), see Figure 4.6. However, the fact that $\gamma_\pm$ are globally constant is a more subtle issue that is related to the periodicity of the curvature of $\Lambda_\mathrm{h}(L;\mu)$, i.e. to the 'belly dance'.

In Figure 4.6 we plot the spectral curves $\Lambda_\mathrm{h}(L) = \{\lambda_\mathrm{Ho}(\gamma, k) : \gamma \in \mathbb{S}^1\}$ for the six values of k marked by the vertical lines in Figure 4.5(a). We also indicate the '+1' endpoints, i.e, $\lambda_\mathrm{Ho}(+1, k)$. Curve 1 of Figure 4.6 touches the imaginary axis at $\gamma = +1$ for the k value slightly above the first crossing of the two Hopf curves. Curve 2 is slightly below this value of k and here the '+1' end lies in the open left half plane while $\lambda^+_\mathrm{Ho}(-1, k)$ touches the imaginary axis. Comparing curves 1 and 2 we notice an overall counter-clockwise rotation. This rotation continues as k is decreased further, and at the same time the curve of spectrum straightens while decreasing in length, see curves 3 and 4. Curves 5 and 6 are already very small, and hence magnified in the inset. Note that curve 6 is similar to curve 1 only the linear wavenumbers $\gamma = \pm 1$ of the endpoints are interchanged. Up to this change, the picture for the next two intersections is qualitatively the same. In particular, the curvature of $\lambda^+_\mathrm{Ho}(\gamma, k)$ changes sign so that most unstable point of this part of the spectrum is either $\lambda^+_\mathrm{Ho}(+1, k)$ or $\lambda^+_\mathrm{Ho}(-1, k)$. We corroborated this by computing the curve in the (A, k)-parameter plane for which $\lambda_\mathrm{Ho}(\mathrm{i}, A, k) \in \mathrm{i}\mathbb{R}$, that is, where a representative point inside the

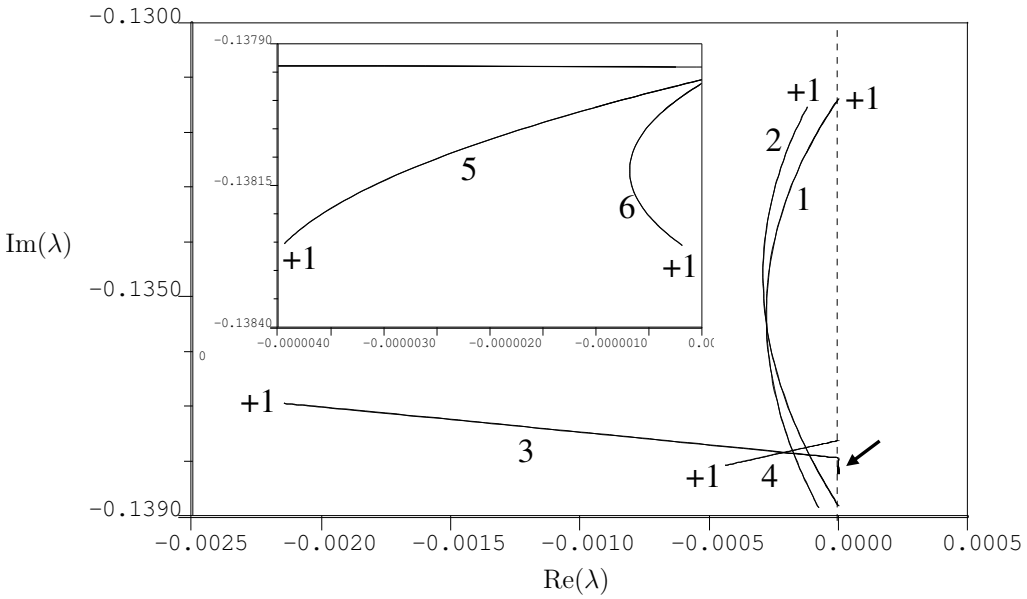

Figure 4.6: The spectral curves $\lambda_{\mathrm{Ho}}(\gamma, k)$, with '+1' denoting $\lambda_{\mathrm{Ho}}(+1, k)$, for the six values of k marked in Figure 4.5(a) using the same labels. The inset enlarges the region near the arrow head.

'belly' of the curve of spectrum lies on the imaginary axis. We find that for given k it has $A \leq \max(A_{\pm}(k))$ so that it always lies in the unstable region. We discuss more details of this belly dance in the next subsection.

4.3.4 The belly dance

As mentioned several times before, the fact that the $\mathcal{H}_{\pm 1}$ curves always yield the entire stability boundary is related to the change in curvature of the critical branch of spectral curve associated to the Hopf destabilization. Instead of investigating this along the stability boundary, we consider here A fixed at 0.01 and compare $\lambda_{\mathrm{Ho}}(\gamma, 0.01, k)$ for $\gamma \in \{+1, \mathrm{i}, -1\}$ as k decreases. For convenience we denote

$$\lambda_*(\gamma, L) := \lambda^+_{\mathrm{Ho}}(\gamma, 0.01, 2\pi/L).$$

We observe the same rotation and geometry as in Figure 4.6, but this choice of curve simplifies some of the computations. In Figure 4.7(a), we plot the two curves

$$\mathrm{Re}(\lambda_*(+1, L) - \lambda_*(-1, L)) \exp(0.253L), \quad \mathrm{Re}(\lambda_*(\mathrm{i}, L) - \lambda_*(-1, L)) \exp(0.253L), \tag{3.1}$$

in blue and red, respectively. We obtain a periodic graph up to an exponential factor, and infer that $\lambda_*(\mathrm{i}, L)$ is always more stable than either $\lambda_*(+1, L)$ or $\lambda_*(-1, L)$. This

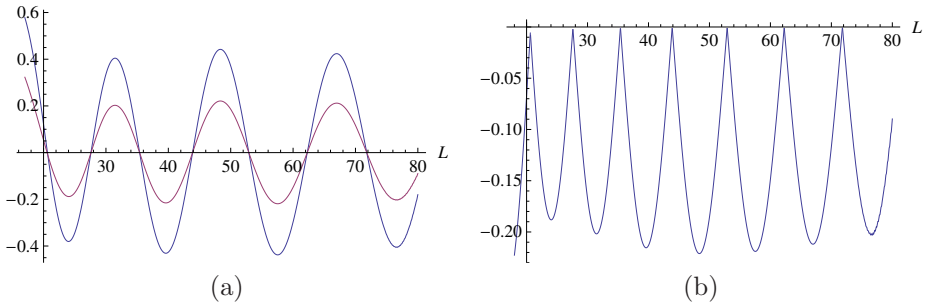

(a) (b)

Figure 4.7: (a) Plot of the two graphs of (3.1); the first in blue, the second in red. (b) Plot of the graph of (3.2).

is further illustrated in Figure 4.7(b) where we plot

$$(\mathrm{Re}(\lambda_*(i,L) - \max\{\mathrm{Re}(\lambda_*(\gamma,L)) : \gamma = \pm 1\})\exp(0.253L), \tag{3.2}$$

which clearly always is negative. Geometrically, the line connecting $\lambda_*(+1,L)$ with $\lambda_*(-1,L)$, i.e. the leading order approximation of the entire spectral curve, is vertical at the roots of the blue curve in Figure 4.7(a). This occurs at every half-cycle of the rotation of the curve of spectrum as considered in Figure 4.6. Figure 4.7(b) establishes that at these values of L the point $\lambda_*(\mathrm{i},L)$ lies to the left of this line in the complex plane. In other words, the belly of the spectral curves always points into the stable half plane. In fact, this also implies that the belly oscillates with twice the frequency of the rotation of the spectral curve (which can also checked directly from the numerical data). These numerical findings are all once more confirmed by the analysis of the normal form model presented in section §4.5.2 and especially in Figure 4.9.

4.3.5 Relation to the literature and to the normal form

In order to relate the computations presented in this section to the analytical literature on the Gray-Scott model (see for instance [16, 18, 48, 49, 56, 58]), we first need to decide upon the asymptotic magnitudes of parameters A and B with respect to ε. Since $\varepsilon^4 = 0.001$, i.e. $\varepsilon \approx 0.18$, and $B = 0.26$, it is natural to set $B = b\varepsilon$ with $b \approx 1.46$. An overlap between our computations and the analytical literature is formed by the (de)stabilization of homoclinic and nearly-homoclinic patterns, i.e. patterns with $k = 0$, or close to 0. Since the curve sn_2 represents the onset of pulse self-replication, see §4.3.1, which is known to be (just) outside the region of asymptotic analysis [16, 48, 57], we need to focus on the curves sn_1 and $\mathcal{H}_{\pm 1}$ in the (inset of) Figure 4.2(a) near $k = 0$. Since $\varepsilon^4 = 0.001$, it is thus natural to scale A as $a\varepsilon^4$.

As for the general model (1.5), the pulses in the Gray-Scott model do not have a $\mathcal{O}(1)$ amplitude. Following [16, 18], and as we did in §4.1.2, we scale U and V in (1.1), $\tilde{U} = U/(\varepsilon\sqrt{\varepsilon})$, $\tilde{V}(x,t) = \sqrt{\varepsilon}V$. Moreover, we introduce $\tilde{t} = \varepsilon$ and $\tilde{x} = x/\sqrt{\varepsilon}$

and obtain (after dropping all tildes),

$$\left\{\begin{array}{rcrcrcl} \varepsilon^2 U_t &=& U_{xx} &-& a\varepsilon^3\sqrt{\varepsilon}(1-\varepsilon\sqrt{\varepsilon}U) &-& UV^2 \\ V_t &=& \varepsilon^2 V_{xx} &-& bV &+& UV^2 \end{array}\right. . \tag{3.3}$$

This version of the Gray-Scott model is very similar to (1.4) and therefore suitable to explain the differences between the Gray-Scott model in the parameter range considered here and the normal form model. Of course, an a priori important difference is the fact that the background state in (1.1) or (3.3) is not $(U(x,t),V(x,t)) \equiv (0,0)$. This is – however – not significant. The fact that the slow component does not remain $\mathcal{O}(1)$ in between two 'fast' V-pulses is much more relevant: in (3.3) it varies from being $\mathcal{O}(1)$ near a fast pulse to $\mathcal{O}(1/(\varepsilon\sqrt{\varepsilon}))$ in between two fast pulses (hence the scaling of $\tilde{U}$). Moreover, the linear term in the U-equation is not of $\mathcal{O}(\varepsilon^2)$, but smaller, $\mathcal{O}(\varepsilon^3\sqrt{\varepsilon})$.

Together, these two differences between (3.3) and (1.4) have as effect that the distance between two successive fast V-pulses is much longer in (3.3) than in (1.4). In (1.4), $U_{xx} = \varepsilon^2 U$ between two fast (stationary) pulses (V is exponentially small). Since the total variation in U is $\mathcal{O}(1)$, this implies that the natural wavelength of periodic patterns is $\mathcal{O}(1/\varepsilon)$ – i.e. $\mathcal{O}(1/\varepsilon^2)$ in the fast spatial scale ξ, see §4.4 and especially Theorem 4.1. In contrast, in the normalized Gray-Scott model (3.3), $U_{xx} = \varepsilon^{7/2}U$ to leading order, while the variation in U must be $\mathcal{O}(\varepsilon^{-3/2})$, hence the wavelength is of a periodic pattern in (3.3) is $\mathcal{O}(\varepsilon^{-5/2}) \gg O(\varepsilon^{-1})$.

Thus, the Gray-Scott model (3.3) is singular in the sense that the wavelength of 'typical' periodic patterns is much larger than in the 'normal' case (1.4). As a consequence, the length of the spectral branches Λ associated to the stability of the periodic patterns is much smaller than in the normal case, see §4.4 and §4.5. In fact, the branches Λ_{h}, i.e. the ones that are responsible for the Hopf dance (§4.5), are not of $\mathcal{O}(1)$ (as is the case for (1.4)), but asymptotically small in ε. In the Evans function approach to the stability of singular spatially periodic patterns developed in [68], the effect of the higher order corrections has been proved to be asymptotically small, and thus no attention has been paid to the higher order terms. However, this means that in the context of the 'singular' Gray-Scott model (3.3), the approach of [68] only gives the leading order position of the branch Λ_{h} as a point (a point that was already determined by the formal analysis presented in [16]). Thus, the leading order methods of [68] do not give any information on the geometry of the spectral branch Λ_{h} for the 'singular' Gray-Scott system, contrary to the 'normal' system (1.4) in which both the Hopf dance and the belly dance can be deduced analytically from the general frame work developed in [68].

The fact that the singular Gray-Scott system nevertheless exhibits the same Hopf dance behavior as the normal form model is another strong indication that the Hopf dance, i.e. snaking of the two Hopf bifurcation curves $\mathcal{H}_{\pm 1}$ near the homoclinic tip of a Busse balloon, indeed is a very robust phenomenon.

Remark 3.2 We refer to [16, 56, 48, 49] for analytical results on the existence and stability of spatially periodic patterns in the Gray-Scott model and their relations with explicit numerical simulations.

4.4 Preliminaries II: Periodic patterns in the normal form model (1.4)

In this section, we formulate the results on the existence and stability of a (class of) periodic pattern solutions to (1.4) that have originally been obtained in [22] and [68].

4.4.1 The existence of periodic pulse patterns

Stationary spatially periodic patterns in (1.4) correspond to periodic solutions in the 4-dimensional system,

$$\left\{\begin{array}{lcl} \dot{u} &=& \varepsilon p \\ \dot{p} &=& -\varepsilon u^{\alpha_1} v^{\beta_1} + \varepsilon^3 \mu u \\ \dot{v} &=& q \\ \dot{q} &=& v - u^{\alpha_2} v^{\beta_2} \end{array}\right. \tag{4.1}$$

where the dot denotes the derivative with respect to the fast spatial coordinate $\xi = x/\varepsilon$. The fast reduced limit,

$$u = \bar{u},\ p = \bar{p},\ \ddot{v} = v - \bar{u}^{\alpha_2} v^{\beta_2},$$

has the homoclinic solution,

$$v_{\rm h}^r(\xi;\bar{u}) = \bar{u}^{-\frac{\alpha_2}{\beta_2-1}} w_{\rm h}^r(\xi) \ \text{ with } \ w_{\rm h}^r(\xi) = \left(\frac{\beta_2+1}{2}\right)^{\frac{1}{\beta_2-1}} \left(\operatorname{sech}\left(\frac{1}{2}(\beta_2-1)\xi\right)\right)^{\frac{2}{\beta_2-1}}. \tag{4.2}$$

For large ξ, v and $q = \dot{v}$ are exponentially small. In that case, the (spatial) dynamics are driven by the (linear) slow reduced system,

$$v = q = 0,\ \ddot{u} = \varepsilon^4 \mu u. \tag{4.3}$$

We can now state the main existence theorem, where we introduce the parameter $\ell = \varepsilon^2 L$.

Theorem 4.1 [22] *Let $\mu, \alpha_1, \alpha_2, \beta_1, \beta_2$ satisfy (1.8). Then, there is an $\varepsilon_0 > 0$ such that for all $0 < \varepsilon < \varepsilon_0$, (4.1) possesses a family of periodic orbits $\gamma_{\rm p}(\xi; L)$ parametrized by their wavelength $L \stackrel{\rm def}{=} 2\ell/\varepsilon^2$, with*

$$\ell \in [\ell_{\rm sn}, \infty) \ \text{ and } \ \ell_{\rm sn} = \frac{1}{\sqrt{\mu}} \operatorname{arccosh} \sqrt{\frac{\beta_2 - 1 + d}{d}} + \mathcal{O}(\varepsilon)$$

(1.7), (1.8). The solutions $\gamma_{\rm p}(\xi; L)$ have positive $u_{\rm p}$- and $v_{\rm p}$-coordinates and two internal reflection symmetry points at distance $L = 2\ell/\varepsilon^2$ apart (in ξ) at which $p_{\rm p} =$

$q_{\rm p} = 0$. *They consist of a slow pieces on which* $\gamma_{\rm p}(\xi; L)$ *is exponentially close to a* cosh*-type solution of (4.3), alternated by fast parts in which* $\gamma_{\rm p}(\xi; L)$ *is* $\mathcal{O}(\varepsilon)$ *close to* $(\bar{u}_\ell, 0, v_{\rm h}^r(\xi; \bar{u}_\ell), \dot{v}_{\rm h}^r(\xi; \bar{u}_\ell))$ *(4.2), with*

$$\bar{u}_\ell = (2\sqrt{\mu}\tanh\sqrt{\mu}\ell)^{\frac{\beta_2-1}{d}} \left(\int_{-\infty}^{\infty} (w_{\rm h}^r(\xi))^{\beta_1} d\xi\right)^{-\frac{\beta_2-1}{d}}.$$

In the limit $\ell \to \infty$, $\gamma_{\rm p}(\xi; L)$ *merges with the solution* $\gamma_{\rm h}(\xi)$ *that is homoclinic to* $(0,0,0,0)$*;* $\gamma_{\rm p}(\xi; L)$ *undergoes a saddle node bifurcation at* $\ell = \ell_{\rm sn}$.

The orbits $\gamma_{\rm p}(\xi; L)$ *correspond to a family of stationary, symmetric, spatially periodic patterns* $(U_{\rm p}(\xi; L), V_{\rm p}(\xi; L))$ *in (1.4) parametrized by their wavelength* L.

This theorem is proved in [22] by the methods of geometric singular perturbation theory. It should be noted that there are many more families of periodic patterns in (1.4), see [22]. The patterns $(U_{\rm p}(\xi; L), V_{\rm p}(\xi; L))$ described here correspond to the A-type patterns studied in [68] and are the only periodic patterns among those constructed in [22] that may be stable as solutions of (1.4) [68]. Except for the obvious fact that the slow cosh-type U-pieces have their minimums (and not their maximums) in between two successive fast V-pulses, the $(U_{\rm p}(\xi; L), V_{\rm p}(\xi; L))$-patterns are very similar to the Gray-Scott patterns presented in Figure 4.1.

4.4.2 Stability by the Evans function approach

The spectral stability analysis of the periodic patterns $(U_{\rm p}(\xi; L), V_{\rm p}(\xi; L))$ given by Theorem 4.1 completely follows the lines sketched in §4.2. Thus, the stability is determined by an Evans function $\mathcal{D}(\lambda, \gamma; L)$. Based on the direct linearization of (1.4) about the periodic pattern $(U_{\rm p}(\xi; L), V_{\rm p}(\xi; L))$ of Theorem 4.1 in the fast spatial coordinate ξ,

$$\begin{cases} u_{\xi\xi} = -\varepsilon^2 \left[\alpha_1 U_{\rm p}^{\alpha_1-1} V_{\rm p}^{\beta_1} u + \beta_1 U_{\rm p}^{\alpha_1} V_{\rm p}^{\beta_1-1} v\right] + \varepsilon^4 (\mu+\lambda)\, u \\ v_{\xi\xi} + \left[\beta_2 U_{\rm p}^{\alpha_2} V_{\rm p}^{\beta_2-1} - (1+\lambda)\right] v = -\alpha_2 U_{\rm p}^{\alpha_2-1} V_{\rm p}^{\beta_2} u \end{cases}, \tag{4.4}$$

the spectral problem can be written in the form (2.2). As for the existence problem, a central role is played by the fast reduced limit problem associated to (4.4),

$$u \equiv \hat{u}, \;\; v_{\xi\xi} + \left[\beta_2 (w_{\rm h}^r(\xi))^{\beta_2-1} - (1+\lambda)\right] v = -\alpha_2 \hat{u} (\bar{u}_\ell)^{-\frac{\alpha_2+\beta_2-1}{\beta_2-1}} (w_{\rm h}^r(\xi))^{\beta_2}, \tag{4.5}$$

that is obtained by taking the limit $\varepsilon \to 0$ in (4.4) using (4.2) and Theorem 4.1. We denote

$$\mathcal{L}(\xi; \beta_2) = \beta_2 (w_{\rm h}^r(\xi))^{\beta_2-1} - 1.$$

Since (4.4) is a linear problem, we can choose the value of $\hat{u}$ (by scaling). There are only two significant choices possible, $\hat{u} = 0$, or $\hat{u} = 1$. In the former case, (4.5) corresponds to the stability of the singular pulse solution $v_{\rm h}^r(\xi; \bar{u}_\ell)$ (4.2) as solution to the scalar reduction of (1.4) in the fast field, $V_t = V_{\xi\xi} - V + \bar{u}_\ell^{\alpha_2} V_2^{\beta}$. This problem, $(\mathcal{L}(\xi; \beta_2) - \lambda)v = 0$, has essentially been solved in [17]: there are $J+1$ eigenvalues

$\lambda_j^r = \lambda_j^r(\beta_2)$, $j = 0, ..., J$, with $\lambda_0^r = \frac{1}{4}(\beta_2 - 1)^2 - 1$, $\lambda_1^r \equiv 0$, $\lambda_j^r \in (-1, 0)$ for $j \geq 2$ and $\lambda_{j+1}^r < \lambda_j^r$. Moreover, the general solutions, and thus the eigenfunctions $v_j^r(\xi)$ for $\lambda = \lambda_j^r$, can be determined explicitly; there also is an explicit expression for $J = J(\beta_2)$ [17]. This also means that the Evans function associated to this problem, which we denote here in terms of a transmission function $t_f(\lambda)$, can be considered as a known expression [17].

If $\hat{u} \neq 0$, we scale it to 1 and introduce $w_{\rm in}(\xi; \lambda)$ as the bounded solution of the inhomogeneous problem,

$$(\mathcal{L}(\xi; \beta_2) - \lambda)w = (w_{\rm h}^r(\xi))^{\beta_2}, \tag{4.6}$$

which is obtained from (4.5) by an appropriate scaling of v. Note that $w_{\rm in}(\xi; \lambda) = (\mathcal{L}(\xi; \beta_2) - \lambda)^{-1}(w_{\rm h}^r(\xi))^{\beta_2}$ is uniquely determined for $\lambda \neq \lambda_j^r$ and can be computed explicitly (using the general solutions of the homogeneous problem [17]). Moreover, it is straightforward to show that $\mathcal{L}(\xi; \beta_2) - \lambda$ cannot be inverted for $\lambda = \lambda_j^r$, j even, and that $w_{\rm in}(\xi; \lambda)$ exists, but is non-unique, if $\lambda \neq \lambda_j^r$ and j odd [17].

Finally, we need one additional ingredient to formulate the main result of [68] that describes the spectrum $\sigma((U_{\rm p}, V_{\rm p}))$ associated to the stability of the periodic patterns $(U_{\rm p}(\xi; L), V_{\rm p}(\xi; L))$ of Theorem 4.1: for $\delta > 0$, the region $\mathbb{C}_r \subset \mathbb{C}$ is defined by

$$\mathbb{C}_r(\delta) = \mathbb{C} \backslash \Big\{ \{\lambda \in \mathbb{C} : {\rm Re}[\lambda] < \max(-1, -\mu) + \delta,\ |{\rm Im}[\lambda]| < \delta\} \bigcup \{\cup_{\rm j=0,...,J-1} {\rm B}(\lambda_{\rm j}^{\rm r}, \delta)\} \Big\}. \tag{4.7}$$

Thus, $\mathbb{C}_r$ is $\mathbb{C}$, except for δ-neighborhoods of the reduced eigenvalues λ_j^r and of $\{\lambda \in \mathbb{R} : \lambda < \max(-1, -\mu)\}$ – the spectrum associated to the stability of the trivial state $(0, 0)$ (and thus the essential spectrum of pulse type solutions of (1.4)).

Theorem 4.2 [68] *Let $\mu, \alpha_1, \alpha_2, \beta_1, \beta_2$ satisfy (1.8) and let $\ell > \ell_{\rm sn}$. There is a $\delta_0 > 0$ and an $\varepsilon_0 = \varepsilon_0(\delta) > 0$ such that for all $0 < \delta < \delta_0$ and $0 < \varepsilon < \varepsilon_0(\delta)$, $\mathcal{D}(\lambda, \gamma; L) \neq 0$ for $\lambda \in \{\mathbb{C} \backslash \mathbb{C}_r\} \cap \{{\rm Re}[\lambda] > 0\}$, i.e. there are no unstable γ-eigenvalues outside $\mathbb{C}_r$. For $\lambda \in \mathbb{C}_r$ (and $0 < \delta < \delta_0$, $0 < \varepsilon < \varepsilon(\delta)$), the Evans function $\mathcal{D}(\lambda, \gamma; L)$ associated to the spectral problem (2.2) for the patterns $(U_{\rm p}(\xi; L), V_{\rm p}(\xi; L))$ of Theorem 4.1 can be decomposed into a product of a 'fast' and a 'slow' Evans function,*

$$\mathcal{D}(\lambda, \gamma; L) = \mathcal{D}_f(\lambda, \gamma; L)\mathcal{D}_s(\lambda, \gamma; \ell), \quad \lambda \in \mathbb{C}_r, \gamma \in \mathbb{S}^1,$$

where,

$$\mathcal{D}_f(\lambda, \gamma; L) = -\gamma t_f(\lambda)\, e^{2L\sqrt{1+\lambda}}(1 + \mathcal{O}(\varepsilon)), \tag{4.8}$$

in which $t_f(\lambda)$ is the transmission function associated to the limit problem (4.5) with $\hat{u} = 0$, and,

$$\mathcal{D}_s(\lambda, \gamma; \ell) = \gamma \left[2\gamma_{\rm r} - \left(\frac{1}{E(\lambda, \ell)} t_{11}(\lambda, \ell) + E(\lambda, \ell) t_{22}(\lambda, \ell) + \mathcal{O}(\varepsilon) \right) \right] \tag{4.9}$$

with $\gamma_{\rm r} = {\rm Re}[\gamma] \in [-1, 1]$,

$$E(\lambda, \ell; \mu) = e^{-2\ell\sqrt{\mu+\lambda}} \in \mathbb{C}, \tag{4.10}$$

and $\ell = \frac{1}{2}\varepsilon^2 L = \mathcal{O}(1)$ *as in Theorem 4.1. Moreover,*

$$t_{11}(\lambda, \ell; \mu) = 1 - \mathcal{S}(\lambda; \mu) \tanh \ell\sqrt{\mu}, \;\; t_{22}(\lambda, \ell; \mu) = 1 + \mathcal{S}(\lambda; \mu) \tanh \ell\sqrt{\mu}, \tag{4.11}$$

with the analytic functions (for $\lambda \in \mathbb{C}_r$*),*

$$\mathcal{S}(\lambda; \mu) = \frac{\sqrt{\mu}}{\sqrt{\mu + \lambda}} \left[\alpha_1 - \alpha_2 \beta_1 \mathcal{R}(\lambda)\right], \tag{4.12}$$

and

$$\mathcal{R}(\lambda; \beta_1, \beta_2) = \left(\int_{-\infty}^{\infty} w_{\text{in}}(\xi; \lambda) (w_{\text{h}}^r(\xi))^{\beta_1 - 1} d\xi \right) \Big/ \left(\int_{-\infty}^{\infty} (w_{\text{h}}^r(\xi))^{\beta_1} d\xi \right), \tag{4.13}$$

(4.2), (4.6), that can be computed explicitly [17].

The proof of this result is given in [68]. It is based on the NLEP method developed in [17] for the decomposition and explicit approximation of the Evans function associated to the stability of homoclinic patterns $(U_{\text{h}}(\xi), V_{\text{h}}(\xi))$ in (1.4) that appear as the limit for $L \to \infty$, i.e. $k \downarrow 0$, from the periodic patterns $(U_{\text{p}}(\xi; L), V_{\text{p}}(\xi; L))$ (Theorem 4.1).

Note that $t_f(\lambda) \neq 0$ for $\lambda \in \mathbb{C}_r$ (by the definition of $\mathbb{C}_r$ (4.7)). Thus, it follows from this theorem that the stability of $(U_{\text{p}}(\xi; L), V_{\text{p}}(\xi; L))$ is determined by the solutions $\lambda(\gamma)$ of $\mathcal{D}_s(\lambda, \gamma; \ell) = 0$ (4.9). Moreover, Theorem 4.2 also establishes that the spectrum $\sigma(U_{\text{p}}, V_{\text{p}})$ cannot cross through $\lambda = 0$ as a parameter is varied (since $\mathcal{D}(\lambda, \gamma; L) \neq 0$ for λ in the positive half plane δ-close to 0). Hence, except for the saddle node bifurcation at $\ell = \ell_{\text{sn}}$ (Theoreom 4.1), the pattern $(U_{\text{p}}(\xi; L), V_{\text{p}}(\xi; L))$ can only be (de)stabilized by a Hopf bifurcation. Due to the 'collapsed' character of the spectral branches $\Lambda(L, \mu)$ (§4.2.2), this implies that the ± 1-type Hopf bifurcations will play an important role in the bifurcation analysis of $(U_{\text{p}}(\xi; L), V_{\text{p}}(\xi; L))$, especially near the homoclinic limit.

4.5 Near the homoclinic pulse: patterns with long wavelengths

In this section we consider the stability and bifurcations of the periodic patterns $(U_{\text{p}}(\xi; L), V_{\text{p}}(\xi; L))$ of Theorem 4.1 for $\ell = \varepsilon^2 L$ large. It follows from [36, 77, 78] that for every discrete eigenvalue $\lambda_{\text{h},j} \in \mathbb{C}$ of the spectral stability problem associated to the limiting homoclinic pattern $(U_{\text{h}}(\xi), V_{\text{h}}(\xi)) = (U_{\text{p}}(\xi; \infty), V_{\text{p}}(\xi; \infty))$, there must be a spectral branch $\Lambda_{\text{h}}(L) \in \mathbb{C}$ of the stability problem associated to the periodic pattern $(U_{\text{p}}(\xi; L), V_{\text{p}}(\xi; L))$ that approaches $\lambda_{\text{h},j}$ as $L \to \infty$ (see Remark 5.1). By the results of Theorem 4.2, we can explicitly approximate the branch $\Lambda_{\text{h}}(L)$ for ℓ large, and thus obtain detailed information on the spectrum $\sigma((U_{\text{p}}, V_{\text{p}}))$ for large ℓ.

To investigate the structure of $\Lambda_{\rm h}$ for large ℓ, we introduce a second small parameter, δ, by setting $\ell = \frac{1}{\delta}$ – note that this is a slight abuse of notation, this δ is not related to the δ introduced in Theorem 4.2. We assume that $\delta = \mathcal{O}(1)$ w.r.t. ε, i.e. $0 < \varepsilon \ll \delta \ll 1$. In fact, we will consider all correction terms in ε – see Theorem 4.2 – as higher order effects in this section (and thus not even refer to these terms). Since a central expression as $E(\lambda, \ell; \mu)$ is exponentially small in δ in absolute value (4.10), this implies that we implicitly assume that ε is much smaller than exponentially small terms in δ in the forthcoming analysis. Note that this is mostly a technical issue, it does not influence the essence of our results.

Remark 5.1 In fact, the results in [78] also establish the exponential decay rate of $\sigma((U_{\rm p}, V_{\rm p}))$ as $L \to \infty$. Moreover, in [78] an expansion similar to the forthcoming one is given for the 'small' spectrum $\sigma((U_{\rm p}, V_{\rm p}))$, i.e. the part of the spectrum that is connected to the origin (and thus is associated to the translational eigenvalue $\lambda(+1) = 0$). Here, we consider the part of the spectrum associated to a 'nontrivial' eigenvalue of the homoclinic limit, more specifically, an eigenvalue associated to a Hopf instability.

4.5.1 The Hopf dance

Since $\lambda(\gamma)$ must be a zero of $\mathcal{D}_s(\lambda, \gamma; \ell)$, it follows from the expression (4.9) in Theorem 4.2 that a spectral branch $\Lambda = \{\lambda = \lambda(\gamma) : \gamma \in \mathbb{S}^1\} \in \mathbb{C}$ (§4.2.1) is implicitly determined by

$$t_{11}(\lambda, \ell) = 2\,\gamma_{\rm r} E(\lambda, \ell) - E^2(\lambda, \ell)\, t_{22}(\lambda, \ell), \tag{5.1}$$

(at leading order in ε). By (4.10), this condition reduces to $t_{11}(\lambda, \ell; \mu) = 0$ as $\ell \to \infty$. Moreover, by (4.11),

$$\lim_{\ell \to \infty} t_{11}(\lambda, \ell; \mu) = 1 - \mathcal{S}(\lambda; \mu) = t_2(\lambda; \mu). \tag{5.2}$$

Here $t_2(\lambda; \mu)$ is in fact the slow transmission function that was shown in [17] to govern the stability of the homoclinic pulse pattern $(U_{\rm h}(\xi), V_{\rm h}(\xi))$. Hence, we have explicitly recovered the above mentioned general results of [36, 78]. In fact, we have obtained a bit more: every spectral branch $\Lambda \subset \mathbb{C}_r$, see (4.7), associated to a periodic pattern $(U_{\rm p}(\xi; L), V_{\rm p}(\xi; L))$ limits on a non-zero eigenvalue λ_h associated to the limiting homoclinic pattern $(U_{\rm h}(\xi), V_{\rm h}(\xi))$ as $\ell \to \infty$. Note that it follows from (5.2) that $\mathcal{S}(\lambda_h; \mu) = 1$.

As mentioned above, the homoclinic pulse $(U_{\rm h}(\xi), V_{\rm h}(\xi))$ can only be (de)stabilized by a pair of complex conjugate eigenvalues $\lambda_{\rm h}(\mu), \overline{\lambda_{\rm h}}(\mu) \notin \mathbb{R}$, with by definition $\mathrm{Im}[\lambda_{\rm h}(\mu)] > 0$. At the bifurcation, the pulse must thus be destabilized by a Hopf instability. In this section we study the spectral curves that limit on these Hopf bifurcation eigenvalues for large but bounded ℓ. The associated critical values of parameter μ and $\lambda_{\rm h}$ are defined by,

$$\lambda_{\rm h}(\mu_{\rm H}) = \lambda_{\rm h,H} = i\lambda_{\rm h,H,i} \in i\mathbb{R} \;\text{ with }\; \lambda_{\rm h,H,i} > 0. \tag{5.3}$$

Thus, by definition,

$$\mathcal{S}(\lambda_{\rm h}(\mu);\mu) \equiv 1. \tag{5.4}$$

Since we have assumed that $\ell = \frac{1}{\delta} \gg 1$, it follows that $|E(\lambda,\ell;\mu)|$ is exponentially small in δ (4.10). Therefore, we define

$$E_{\rm h} = E_{\rm h}(\ell;\mu) = E(\lambda_{\rm h},\ell;\mu) = e^{-2\ell\sqrt{\mu+\lambda_{\rm h}}}, \;\; E_0 = E_0(\ell;\mu) = E(0,\ell;\mu) = e^{-2\ell\sqrt{\mu}}. \tag{5.5}$$

and obtain the following expansion,

$$\tanh \ell\sqrt{\mu} = 1 - 2E_0 + 2E_0^2 + \mathcal{O}_E(3), \tag{5.6}$$

where the $\mathcal{O}_E(N)$ notation indicates the order in $|E|$, $\mathcal{O}_E(N) = \mathcal{O}_E(|E|^N)$ – note that this notation is somewhat ambiguous, since the magnitude of $|E|$ strongly depends on the values of λ and μ – see (5.11), (5.12) below. Since we know that λ must be close to $\lambda_{\rm h}$, we expand $\mathcal{S}(\lambda;\mu)$ as a Taylor series in $(\lambda - \lambda_{\rm h})$,

$$\mathcal{S}(\lambda;\mu) = 1 + (\lambda-\lambda_{\rm h})\mathcal{S}'(\lambda_{\rm h};\mu) + \frac{1}{2}(\lambda-\lambda_{\rm h})^2\mathcal{S}''(\lambda_{\rm h};\mu) + \mathcal{O}_E(3), \tag{5.7}$$

where we anticipate the forthcoming result that $\lambda - \lambda_{\rm h} = \mathcal{O}_E(|E|)$. The expression $E(\lambda;\mu)$ can be expanded in terms of both $E_{\rm h}$ and $(\lambda - \lambda_{\rm h})$,

$$E(\lambda,\ell;\mu) = E_{\rm h} - \ell(\lambda-\lambda_{\rm h})\frac{1}{\sqrt{\mu+\lambda_{\rm h}}}E_{\rm h} + \mathcal{O}_E(3), \tag{5.8}$$

where we have implicitly used that $\ell^k|E_{\rm h}^{m+1}| \ll |E_{\rm h}^m|$ for all $k \geq 0$. Substitution of the $\mathcal{O}_E(1)$ parts of these expansions into (5.1), using (4.11), yields a leading order approximation of $\Lambda_{\rm h}$,

$$-(\lambda-\lambda_{\rm h})\mathcal{S}'(\lambda_{\rm h}) + 2E_0 = 2E_{\rm h}\gamma_{\rm r} + \mathcal{O}_E(2).$$

We have thus obtained the following lemma.

Lemma 5.2 *There is a $\delta_0 > 0$ such that for all $\ell > 1/\delta_0$, the spectral branch $\Lambda_{\rm h}(\ell;\mu)$ is given by,*

$$\Lambda_{\rm h}(\ell;\mu) = \left\{ \lambda(\gamma,\ell;\mu) = \lambda_{\rm h}(\mu) + \frac{2}{\mathcal{S}'(\lambda_{\rm h};\mu)}\left(E_0(\ell;\mu) - \gamma_{\rm r}E_{\rm h}(\ell;\mu)\right) + \mathcal{O}_E(2), \gamma \in \mathbb{S}^1 \right\}. \tag{5.9}$$

Thus, to leading order, $\Lambda_{\rm h}(\ell;\mu)$ is a straight interval at a distance of $|2E_0(\ell;\mu)/\mathcal{S}'(\lambda_{\rm h};\mu)|$ from $\lambda_{\rm h}$. Both this distance and the length of the interval decrease exponentially fast with ℓ. The endpoints of $\Lambda_{\rm h}(\ell;\mu)$ are given by

$$\partial_\pm\Lambda_{\rm h}(\ell;\mu) = \lambda_{\rm h}(\mu) + \frac{2}{\mathcal{S}'(\lambda_{\rm h};\mu)}\left(E_0(\ell;\mu) \mp E_{\rm h}(\ell;\mu)\right). \tag{5.10}$$

Recall that $\partial_+\Lambda_{\rm h}(\mu)$ corresponds to the $\mathcal{H}_{+1}-$Hopf bifurcation, in which all extrema of the pattern $(U_{\rm p}(\xi;L), V_{\rm p}(\xi;L))$ start to oscillate exactly in phase at the bifurcation, and $\partial_+\Lambda_{\rm h}(\mu)$ to the $\mathcal{H}_{-1}-$Hopf bifurcation, in which extrema that are one period $(= 2L)$ away from each other begin to oscillate exactly out of phase (§4.2.2).

Remark 5.3 A result similar to Lemma 5.2 has been presented in [68] (Lemma 6.1). However, there the presence of the term $E_0(\ell;\mu)$ in (5.9) has been overlooked.

Next we infer more geometric information about Λ_h. By the lemma, the length of Λ_h is to leading order given by $2|E_\mathrm{h}/\mathcal{S}'|$, and the distance to λ_h is to leading order given by $2|E_0/\mathcal{S}'|$. The relative magnitude of these quantities is thus determined by

$$|E_\mathrm{h}(\ell;\mu)/E_0(\ell;\mu)| = e^{-2\ell\left(\mathrm{Re}\sqrt{\mu+\lambda_\mathrm{h}}-\sqrt{\mu}\right)}, \tag{5.11}$$

which is exponentially small in δ if $\mu > 0$ and $\lambda = \lambda_\mathrm{r} + i\lambda_\mathrm{i}$ are such that

$$2\mu\lambda_\mathrm{r} + \lambda_\mathrm{i}^2 > 0. \tag{5.12}$$

Note that this is satisfied if $\lambda_\mathrm{r} \geq 0$. Since $\lambda_\mathrm{h}(\mu_\mathrm{H}) = i\lambda_{\mathrm{h,H,i}}$ with $\lambda_{\mathrm{h,H,i}} > 0$ due to (5.3), (5.12) also holds near the bifurcation at which $(U_\mathrm{p}(\xi;L), V_\mathrm{p}(\xi;L))$ destabilizes. Hence, near the destabilization, and in general when (5.12) holds, the length of Λ_h is much shorter than its distance to λ_h. On the other hand, the orientation of Λ_h with respect to λ_h is to leading order governed by

$$\frac{E_\mathrm{h}(\ell;\mu)}{\mathcal{S}'(\lambda_\mathrm{h};\mu)} = \frac{e^{-2\ell\nu_{\mathrm{h,r}}}}{\rho_\mathrm{h}}\left[\cos\left(2\ell\nu_{\mathrm{h,i}} - \theta_\mathrm{h}\right) - i\sin\left(2\ell\nu_{\mathrm{h,i}} - \theta_\mathrm{h}\right)\right], \tag{5.13}$$

in which

$$\begin{array}{lcl} \nu_\mathrm{h}(\mu) & \stackrel{\mathrm{def}}{=} & +\sqrt{\mu+\lambda_\mathrm{h}(\mu)} = \nu_{\mathrm{h,r}} + i\nu_{\mathrm{h,i}} \ \text{ with } \ \arg\left[\nu_\mathrm{h}(\mu)\right] \in (0,\pi), \\ \mathcal{S}'(\lambda_\mathrm{h};\mu) & \stackrel{\mathrm{def}}{=} & \rho_\mathrm{h}(\mu)e^{i\theta_\mathrm{h}(\mu)} \ \text{ with } \ \rho_\mathrm{h} \in \mathbb{R}^+, \theta_\mathrm{h} \in [0,2\pi) \end{array} \tag{5.14}$$

(Lemma 5.2). Combined, the above observations imply that

$$\mathrm{Re}[\lambda(\gamma)] \gtrless \mathrm{Re}[\lambda_\mathrm{h}] \ \text{ for all } \ \gamma \in \mathbb{S}^1 \ \Leftrightarrow \ \mathrm{Re}[\mathcal{S}'(\lambda_\mathrm{h};\mu)] \gtrless 0 \tag{5.15}$$

if (5.12) holds – see Figure 4.8. It thus follows that the homoclinic pattern $(U_\mathrm{h}(\xi), V_\mathrm{h}(\xi))$ is the last 'periodic' pattern to destabilize if and only if $\mathrm{Re}[\mathcal{S}'(\lambda_{\mathrm{h,H}};\mu_H)]$, the value of $\mathrm{Re}[\mathcal{S}'(\lambda_\mathrm{h};\mu)]$ at the Hopf bifurcation (5.3), is positive. Or, vice versa, there exist stable periodic patterns $(U_\mathrm{p}(\xi;L), V_\mathrm{p}(\xi;L))$ with $L = 2\ell/\varepsilon^2$ and $\ell = 1/\delta$, when $(U_\mathrm{h}(\xi), V_\mathrm{h}(\xi))$ has already been destabilized if $\mathrm{Re}[\mathcal{S}'(\lambda_{\mathrm{h,H}};\mu_\mathrm{H})] < 0$ – see again Figure 4.8.

Remark 5.4 It has been conjectured by Wei-Ming Ni in [60] that the homoclinic solution $(U_\mathrm{h}(\xi), V_\mathrm{h}(\xi))$ is the last pattern to become unstable in the generalized Gierer-Meinhardt equation (1.4) as μ approaches a Hopf bifurcation value. Here, we have thus shown that Ni's conjecture reduces to a conjecture on the sign of $\mathrm{Re}[\mathcal{S}'(\lambda_{\mathrm{h,H}};\mu_\mathrm{H})]$. It follows from the analysis of the expression $\mathcal{S}'(\lambda_\mathrm{h};\mu)$ in [17] that $\mathrm{Re}[\mathcal{S}'(\lambda_{\mathrm{h,H}};\mu_H)] > 0$ for the classical Gierer-Meinhardt case ($\alpha_1 = 0, \beta_1 = 2, \alpha_2 = -1, \beta_2 = 2$), hence it follows that Ni's conjecture holds for this case. For a general proof of Ni's conjecture one needs to analyse $\mathrm{Re}[\mathcal{S}'(\lambda_{\mathrm{h,H}};\mu_H)]$ as function of the parameters $\alpha_1, \alpha_2, \beta_1, \beta_2$. It is to be expected that one will encounter behavior that differs significantly from

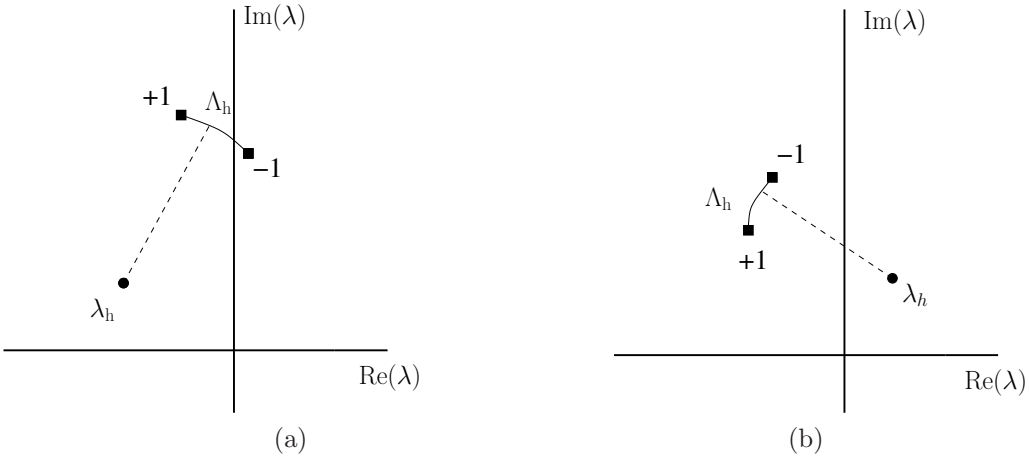

Figure 4.8: (a) A schematic picture of a spectral branch for the case that $\mathrm{Re}[\mathcal{S}'(\lambda_{\mathrm{h,H}};\mu_{\mathrm{H}})] > 0$ for some fixed $\mu > \mu_{\mathrm{H}}$: the homoclinic pattern is the last periodic pattern to destabilizes as $\mu \downarrow \mu_{\mathrm{H}}$. (b) The case that $\mathrm{Re}[\mathcal{S}'(\lambda_{\mathrm{h,H}};\mu_{\mathrm{H}})] < 0$ for some fixed $\mu < \mu_{\mathrm{H}}$: the homoclinic limit is unstable, while there still exist stable long wavelength periodic patterns.

that of the classical case. In fact, in [24] the character of λ_{h} as function of μ for the special case $\alpha_1 = 5/4, \beta_1 = 2, \alpha_2 = -3, \beta_2 = 2$ has been considered (as an example): in this case $\mathrm{Re}[\lambda_{\mathrm{h}}(\mu)]$ changes signs twice as μ increases from 0, i.e. there are two (homoclinic) Hopf bifurcations, at $\mu_{\mathrm{H},1}$ and $\mu_{\mathrm{H},2}$: $(U_{\mathrm{h}}(\xi), V_{\mathrm{h}}(\xi))$ is stable for $\mu \in (\mu_{\mathrm{H},1}, \mu_{\mathrm{H},2})$. It is straightforward to check from the information in [24] that $\mathrm{Re}[\mathcal{S}'(\lambda_{\mathrm{h}}(\mu_{\mathrm{H},1});\mu_{\mathrm{H},1})] > 0$ and $\mathrm{Re}[\mathcal{S}'(\lambda_{\mathrm{h}}(\mu_{\mathrm{H},2});\mu_{\mathrm{H},2})] < 0$. Hence, there still exist stable periodic patterns $(U_{\mathrm{p}}(\xi;L), V_{\mathrm{p}}(\xi;L))$ as $(U_{\mathrm{h}}(\xi), V_{\mathrm{h}}(\xi))$ is destabilized by μ crossing through $\mu_{\mathrm{H},2}$ (in the case $\alpha_1 = 5/4, \beta_1 = 2, \alpha_2 = -3, \beta_2 = 2$). However, this example not necessarily disproves Ni's conjecture, since one could argue that Ni's conjecture concerns only the first bifurcation (for increasing μ) at which stable patterns are created (i.e. $\mu = \mu_{\mathrm{H},1}$ at which $\mathrm{Re}[\mathcal{S}'(\lambda_{\mathrm{h}}(\mu_{\mathrm{H},1});\mu_{\mathrm{H},1})] > 0$).

The Hopf bifurcation curves $\mathcal{H}_{\pm 1} = \{\mu = \mu_{\pm}(\ell) \in \mathbb{C}\}$ are determined by the values of ℓ and μ at which the endpoints $\partial_{\pm}\Lambda_{\mathrm{h}}(\ell;\mu)$ cross through the imaginary axis, i.e. by the condition

$$\mathrm{Re}\left[\partial_{\pm}\Lambda_{\mathrm{h}}(\ell;\mu_{\pm}(\ell))\right] = 0. \tag{5.16}$$

Since we have seen that $\Lambda_{\mathrm{h}}(\ell;\mu)$ is exponentially close to λ_{h}, we expect that both $\mu_{\pm}(\ell)$ are exponentially close – i.e. $\mathcal{O}(|E|) = \mathcal{O}_E(1)$ – to μ_{H} (5.3). Therefore, we expand $\lambda_{\mathrm{h}}(\mu)$ around μ_{H},

$$\lambda_{\mathrm{h}}(\mu) = \lambda_{\mathrm{h,H}} + (\mu - \mu_{\mathrm{H}})\lambda_{\mathrm{h}}'(\mu_{\mathrm{H}}) + \frac{1}{2}(\mu - \mu_{\mathrm{H}})^2\lambda_{\mathrm{h}}''(\mu_{\mathrm{H}}) + \mathcal{O}_E(3), \tag{5.17}$$

once more anticipating on the expectation that $\mu - \mu_{\rm H} = \mathcal{O}_E(1)$. Note that $\lambda_{\rm h}'(\mu_{\rm H})$ and $\lambda_{\rm h}''(\mu_{\rm H})$ can be expressed in terms of $\mathcal{S}'(\lambda_{\rm h,H};\mu_{\rm H})$ and $\mathcal{S}''(\lambda_{\rm h,H};\mu_{\rm H})$ (5.7) by a straightforward expansion of (5.4). For instance,

$$\lambda_{\rm h}'(\mu_{\rm H}) = -\frac{1}{\mathcal{S}'(\lambda_{\rm h,H};\mu_{\rm H})}\frac{\partial \mathcal{S}}{\partial \mu}(\lambda_{\rm h,H};\mu_{\rm H}) = -\frac{1}{2}\frac{\lambda_{\rm h,H}}{\mu_{\rm H}(\mu_{\rm H}+\lambda_{\rm h,H})\mathcal{S}'(\lambda_{\rm h,H};\mu_{\rm H})}, \quad (5.18)$$

where we have used that

$$\frac{\partial \mathcal{S}}{\partial \mu}(\lambda;\mu) = \left[\frac{\partial}{\partial \mu}\frac{\sqrt{\mu}}{\sqrt{\mu+\lambda}}\right]\left[\alpha_1 - \alpha_2\beta_1\mathcal{R}(\lambda)\right] = \frac{1}{2}\frac{\lambda}{\mu(\mu+\lambda)}\mathcal{S}(\lambda;\mu)$$

(4.12), and that $\mathcal{S}(\lambda_{\rm h,H};\mu_{\rm H}) = 1$. The derivation of the expression for $\lambda_{\rm h}''(\mu_{\rm H})$ is similar, but more involved. The combination of (5.17) with Lemma 5.2 (5.9) yields the following leading order approximation of $\Lambda_{\rm h}(\ell;\mu))$ for μ $\mathcal{O}_E(1)$ close $\mu_{\rm H}$,

$$\lambda(\gamma,\ell;\mu) = \lambda_{\rm h,H} + (\mu-\mu_{\rm H})\lambda_{\rm h}'(\mu_{\rm H}) + \frac{2}{\mathcal{S}'(\lambda_{\rm h,H};\mu_{\rm H})}\left(E_0(\ell;\mu_{\rm H}) - \gamma_{\rm r}E_{\rm h}(\ell;\mu_{\rm H})\right) + \mathcal{O}_E(2).$$

The application of condition (5.16) implies that,

$$0 = (\mu_\pm - \mu_{\rm H})\mathrm{Re}\left[\lambda_{\rm h}'(\mu_{\rm H})\right] + \mathrm{Re}\left[\frac{2}{\mathcal{S}'(\lambda_{\rm h,H};\mu_{\rm H})}\left(E_0(\ell;\mu_{\rm H}) \mp E_{\rm h}(\ell;\mu_{\rm H})\right)\right] + \mathcal{O}_E(2),$$

since $\lambda_{\rm h,H} \in i\mathbb{R}$ (5.3). Hence by (5.5) and (5.14),

$$\mu_\pm(\ell) = \mu_{\rm H} - \frac{2}{\mathrm{Re}\left[\lambda_{\rm h}'(\mu_{\rm H})\right]}e^{-2\ell\sqrt{\mu_{\rm H}}}\mathrm{Re}\left[\frac{1 \mp e^{-2\ell((\nu_{\rm h,r}(\mu_{\rm H})-\sqrt{\mu_{\rm H}})+i\nu_{\rm h,i}(\mu_{\rm H}))}}{\mathcal{S}'(\lambda_{\rm h,H};\mu_{\rm H})}\right] + \mathcal{O}_E(2),$$

where $\lambda_{\rm h}'(\mu_{\rm H})$ is determined by (5.18). The above analysis can be summarized as follows.

Corollary 5.5 *There is a $\delta_0 > 0$ such that for all $\ell > 1/\delta_0$, the Hopf bifurcation curves $\mathcal{H}_{\pm 1}$ are to leading order given by*

$$\mu_\pm(\ell) = \mu_{\rm H} - \frac{2}{\rho_{\rm h}(\mu_{\rm H})\mathrm{Re}\left[\lambda_{\rm h}'(\mu_{\rm H})\right]}e^{-2\ell\sqrt{\mu_{\rm H}}}\left[\cos\theta_{\rm h}(\mu_{\rm H}) \mp e^{-2\ell(\nu_{\rm h,r}(\mu_{\rm H})-\sqrt{\mu_{\rm H}})}\cos\left(2\ell\nu_{\rm h,i}(\mu_{\rm H}) - \theta_{\rm h}(\mu_{\rm H})\right)\right].$$

with $\rho_{\rm h}(\mu), \theta_{\rm h}(\mu), \nu_{\rm h,r}(\mu)$, and $\nu_{\rm h,i}(\mu)$ as defined in (5.14) and $\lambda_{\rm h}'(\mu_{\rm H})$ given by (5.18). The curves $\mathcal{H}_{\pm 1}$ 'snake' among each other and have infinitely many intersection points as $\ell \to \infty$ that accumulate on $\mu_{\rm H}$. These intersection points represent co-dimension 2 bifurcations, they are given by $\mu = \mu_{+1}(\ell_2(k)) = \mu_{-1}(\ell_2(k))$ with

$$\ell_2(k) = \frac{\pi + 2\theta_{\rm h}(\mu_{\rm H})}{4\nu_{\rm h,i}(\mu_{\rm H})} + \frac{\pi}{2\nu_{\rm h,i}(\mu_{\rm H})}k > \frac{1}{\delta_0}, \quad k \in \mathbb{N}.$$

Thus this corollary confirms the structure of the the sinusoidally oscillating and exponentially converging snaking curves $\mathcal{H}_{+1}$ and $\mathcal{H}_{-1}$ as found numerically for the Gray-Scott problem in section §4.3.

It should be noted that one could also define the curves $\mathcal{H}(\gamma)$, $\gamma \in \mathbb{S}^1$, that describe the relation between μ and ℓ for which the point $\lambda(\gamma)$ on the spectral branch $\Lambda_{\rm h}(\ell;\mu)$ crosses the imaginary axis (5.9). It is straightforward to check that these curves are all inside the (infinitely many) regions bounded by $\mathcal{H}_{\pm 1}$. This implies that neither of these curves can correspond to a (de)stabilizing Hopf bifurcation, and thus reconfirms the fact that all bifurcations near $\mu_{\rm H}$ must be of $\mathcal{H}_{\pm 1}-$type. Moreover, it also implies that *all* $\mathcal{H}(\gamma)$ curves pass through the co-dimension 2 intersection points determined by $\mathcal{H}_{+1} \cap \mathcal{H}_{-1}$. This is of course a very degenerate but also artificial phenomenon, it is caused by the fact that the spectral branch $\Lambda_{\rm h}(\ell;\mu)$ is *to leading order* a straight interval that coincides with the imaginary axis at the intersection points $\mathcal{H}_{+1} \cap \mathcal{H}_{-1}$. A more accurate approximation of $\Lambda_{\rm h}(\ell;\mu)$ will show that it is in general bent, as we shall show in the upcoming section. Note that the orientation of the associated 'belly' with respect to the imaginary axis decides whether the pattern $(U_{\rm p}(\xi;L), V_{\rm p}(\xi;L))$ indeed may undergo a co-dimension 2 bifurcation caused by both $\mathcal{H}_{+1}$ and $\mathcal{H}_{-1}$, or whether there is no co-dimension 2 bifurcation since it is preceded by and 'interior' $\mathcal{H}(\gamma)-$bifurcation, as described in §4.2.2.

4.5.2 The effect of bending: the belly dance

To study the next order parabolic correction to $\Lambda_{\rm h}(\ell;\mu)$, we need to determine the next order correction to expression (5.9) in Lemma 5.2. As in §4.5.1, we first consider the spectral branch $\Lambda_{\rm h}(\ell;\mu)$ for general μ, i.e. μ not necessarily close to $\mu_{\rm H}$. By (4.10), (5.8), (4.11), (5.6), (5.7),

$$E^2(\lambda,\ell;\mu)\, t_{22}(\lambda,\ell;\mu,0) = [E_{\rm h}(\ell;\mu)+\mathcal{O}_E(2)]^2[1+(1+\mathcal{O}_E(1))(1+\mathcal{O}_E(1))] = 2E_{\rm h}^2(\ell;\mu)+\mathcal{O}_E(3),$$

and we thus find as next order approximation to (5.1),

$$\begin{aligned} -(\lambda-\lambda_{\rm h})\mathcal{S}'(\lambda_{\rm h}) &= 2\gamma_{\rm r}E_{\rm h} - 2E_0 - \tfrac{1}{2}(\lambda-\lambda_{\rm h})^2\mathcal{S}''(\lambda_{\rm h};\mu) - 2E_0(\lambda-\lambda_{\rm h})\mathcal{S}'(\lambda_{\rm h}) \\ &\quad + 2E_0^2 - 2(\lambda-\lambda_{\rm h})\tfrac{\ell}{\sqrt{\mu+\lambda_{\rm h}}}E_{\rm h} - 2E_{\rm h}^2 + \mathcal{O}_E(3), \end{aligned}$$

where we have once again used (4.10), (4.11), (5.6), (5.7), and (5.8). We can now substitute the leading order approximation of $(\lambda-\lambda_{\rm h})$ (5.9) into the right hand side of this identity, to obtain

$$\begin{aligned} (\lambda-\lambda_{\rm h})\mathcal{S}'(\lambda_{\rm h}) &= 2(E_0-\gamma_{\rm r}E_{\rm h}) + 2(E_{\rm h}^2-E_0^2) + 4\tfrac{\ell}{\mathcal{S}'(\lambda_{\rm h})\sqrt{\mu+\lambda_{\rm h}}}\gamma_{\rm r}E_{\rm h}(E_0-\gamma_{\rm r}E_{\rm h}) \\ &\quad + 4E_0(E_0-\gamma_{\rm r}E_{\rm h}) - 2\tfrac{\mathcal{S}''(\lambda_{\rm h})}{(\mathcal{S}'(\lambda_{\rm h}))^2}(E_0-\gamma_{\rm r}E_{\rm h})^2 + \mathcal{O}_E(3). \end{aligned}$$

We have thus obtained,

Lemma 5.6 *There is a $\delta_0 > 0$ such that for all $\ell > 1/\delta_0$, the spectral branch $\Lambda_{\rm h}(\ell;\mu)$ is given by the quadratic approximation,*

$$\Lambda_{\rm h}(\ell;\mu) = \left\{\lambda(\gamma,\ell;\mu) = \lambda_{\rm h}(\mu) + \mathcal{G}_0(\ell;\mu) + \mathcal{G}_1(\ell;\mu)\,\gamma_{\rm r} + \mathcal{G}_2(\ell;\mu)\,\gamma_{\rm r}^2 + \mathcal{O}_E(3), \gamma \in \mathbb{S}^1\right\}, \tag{5.19}$$

with

$$\begin{aligned}
\mathcal{G}_0(\ell;\mu) &= \tfrac{2}{\mathcal{S}'(\lambda_{\rm h})}\left[E_0 + \left(1 - \tfrac{\mathcal{S}''(\lambda_{\rm h})}{(\mathcal{S}'(\lambda_{\rm h}))^2}\right)E_0^2 + E_{\rm h}^2\right] + \mathcal{O}_E(3),\\
\mathcal{G}_1(\ell;\mu) &= -\tfrac{2}{\mathcal{S}'(\lambda_{\rm h})}\left[1 + 2\left(1 - \tfrac{\ell}{\mathcal{S}'(\lambda_{\rm h})\sqrt{\mu+\lambda_{\rm h}}} - \tfrac{\mathcal{S}''(\lambda_{\rm h})}{(\mathcal{S}'(\lambda_{\rm h}))^2}\right)E_0\right]E_{\rm h} + \mathcal{O}_E(3),\\
\mathcal{G}_2(\ell;\mu) &= -\tfrac{2}{(\mathcal{S}'(\lambda_{\rm h}))^2}\left[\tfrac{2\ell}{\sqrt{\mu+\lambda_{\rm h}}} + \tfrac{\mathcal{S}''(\lambda_{\rm h})}{\mathcal{S}'(\lambda_{\rm h})}\right]E_{\rm h}^2 + \mathcal{O}_E(3).
\end{aligned} \tag{5.20}$$

Of course, $\Lambda_{\rm h}(\ell;\mu)$ is at leading order still an interval that rotates as function of ℓ, its rotation is to leading order still determined by (5.13). Nevertheless, as function of $\gamma_{\rm r} \in [-1,1]$, $\Lambda_{\rm h}(\ell;\mu)$ is a parabola (up to corrections of $\mathcal{O}_E(3)$). Moreover, up to a non-rotating factor, the orientation of the parabolic belly is to leading order determined by,

$$\left(\frac{E_{\rm h}(\ell;\mu)}{\mathcal{S}'(\lambda_{\rm h};\mu)}\right)^2 = \frac{e^{-4\ell\nu_{\rm h,r}}}{\rho_{\rm h}^2}\left[\cos\left(4\ell\nu_{\rm h,i} - 2\theta_{\rm h}\right) - i\sin\left(4\ell\nu_{\rm h,i} - 2\theta_{\rm h}\right)\right].$$

(5.20). Thus, the parabolic belly indeed 'dances' around the leading order linear approximation of $\Lambda_{\rm h}(\ell;\mu)$ with a frequency that is twice the frequency of the rotation of $\Lambda_{\rm h}(\ell;\mu)$ (5.13). More precisely: in a coordinate frame that rotates along with the linear leading order approximation so that $\Lambda_{\rm h}(\ell;\mu)$ remains vertical, the $\mathcal{O}_E(2)$ parabolic correction indeed performs a 'belly dance' from left to right. This is in full agreement with the numerical observations for the Gray-Scott model in section §4.3.

In general, the parabolic correction will not have an influence on the destabilization of the periodic pattern $(U_{\rm p}(x;L), V_{\rm p}(x;L))$, it will be caused by one of the endpoints $\partial_\pm\Lambda_{\rm h}(\ell;\mu) = \lambda(\pm1,\ell;\mu)$ (5.19), (5.10). However, near the co-dimension 2 points, where $\Lambda_{\rm h}(\ell;\mu)$ is almost vertical and $\mathrm{Re}[\partial_+\Lambda_{\rm h}(\ell;\mu)]$ and $\mathrm{Re}[\partial_-\Lambda_{\rm h}(\ell;\mu)]$ are close to 0, the parabolic 'belly' may play a role: the orientation of the parabola with respect to the imaginary axis determines whether and endpoint $\partial_\pm\Lambda_{\rm h}(\ell;\mu)$ is the first to cross through the imaginairy axis, or an interior point. Note that $\Lambda_{\rm h}(\ell;\mu)$ would be tangent to the imaginary axis in this latter case, i.e. $\mathrm{Re}[\lambda(\gamma_{\rm r}^{\rm int},\ell;\mu)] = 0$ for some $\gamma_{\rm r}^{\rm int} \neq \pm1$, while $\mathrm{Re}[\lambda(\gamma_{\rm r}^{\rm int},\ell;\mu)] < 0$ for all $\gamma_{\rm r} \in [-1,+1]\backslash\{\gamma_{\rm r}^{\rm int}, \overline{\gamma_{\rm r}}^{\rm int}\}$. However, this does not happen.

Corollary 5.7 *Let $(U_{\rm p}(x;L), V_{\rm p}(x;L))$ be a periodic pattern, let $\ell = \varepsilon^2 L = 1/\delta$ be large enough, and assume that $(U_{\rm p}(x;L), V_{\rm p}(x;L))$ is destabilized by $\Lambda_{\rm h}(\ell;\mu)$ as μ crosses through the critical value $\mu_{\rm dest} = \mu_{\rm dest}(\ell)$. This destabilization either is a Hopf bifurcation of $\mathcal{H}_{+1}-$ or $\mathcal{H}_{-1}-$type, i.e. the destabilization must be caused by one of the endpoints $\partial_\pm\Lambda_{\rm h}(\ell;\mu)$, or it is a co-dimension 2 bifurcation, i.e. $\mu_{\rm dest}$ corresponds to an intersection of the $\mathcal{H}_{+1}-$ and $\mathcal{H}_{-1}-$curves.*

Note that this corollary establishes that the boundary of the Busse balloon near a homoclinic tip indeed must be formed by the two 'snaking' $\mathcal{H}_{+1}-$ and $\mathcal{H}_{-1}-$curves – see Figure 4.10(a).

Since the parabolic correction to $\Lambda_{\rm h}(\ell;\mu)$ only is of $\mathcal{O}_E(2)$ (Lemma 5.6), $(U_{\rm p}(x;L),V_{\rm p}(x;L))$ must be destabilized by a Hopf bifurcation of $\mathcal{H}_{\pm 1}-$type if $\Lambda_{\rm h}(\ell;\mu)$ is not $\mathcal{O}_E(1)$ close to being vertical. The corollary can thus be proved by only considering the near-vertical case, with $\Lambda_{\rm h}(\ell;\mu)$ in the stable part of the complex plane. It will be shown that in this case the parabolic belly is pointing away from the imaginary axis.

Proof. In leading order, the orientation of $\Lambda_{\rm h}(\ell;\mu)$ is determined by (5.9) and especially by (5.13). It follows that $\Lambda_{\rm h}(\ell;\mu)$ is vertical up to $\mathcal{O}_E(1)$ corrections if

$$\frac{E_{\rm h}(\ell;\mu)}{\mathcal{S}'(\lambda_{\rm h};\mu)} = i\mathcal{Q} + \mathcal{O}_E(1), \mathcal{Q}\in\mathbb{R}\ (\mathcal{Q}\neq 0),$$

Thus, by (5.13), $2\ell\nu_{\rm h,i} - \theta_{\rm h} = \frac{1}{2}\pi + k\pi + \mathcal{O}_E(1)$, with $k\in\mathbb{Z}$ and k large enough. Hence, $\Lambda_{\rm h}(\ell;\mu)$ is to leading order vertical for ℓ $\mathcal{O}_E(1)$ close to

$$\ell_{\rm vert}(\mu) = \frac{\pi + 2\theta_{\rm h}}{4\nu_{\rm h,i}} + \frac{\pi}{2\nu_{\rm h,i}}k. \tag{5.21}$$

By (5.20), (5.13), and (5.21), the quadratic deformation of $\Lambda_{\rm h}(\ell;\mu)$ is determined by $\mathcal{G}_2(\ell_{\rm vert},\mu)\gamma_{\rm r}^2$ (5.19), with

$$\mathcal{G}_2(\ell_{\rm vert},\mu) = \frac{2}{\rho_{\rm h}^2}\left[\frac{2\ell_{\rm vert}}{\sqrt{\mu+\lambda_{\rm h}}} + \frac{\mathcal{S}''(\lambda_{\rm h})}{\mathcal{S}'(\lambda_{\rm h})}\right]e^{-4\ell_{\rm vert}\nu_{\rm h,r}} + \mathcal{O}_E(3), \tag{5.22}$$

The assumption $\ell = \frac{1}{\delta} \gg 1$, implies that the orientation of the parabolic 'belly' with respect to its leading order vertical configuration is determined by the real part of $1/\sqrt{\mu+\lambda_{\rm h}}$.

Since $\mathrm{Im}[\lambda_{\rm h}] > 0$ by definition (5.3), it follows that $\arg[\mu+\lambda_{\rm h}] \in (0,\pi)$, so that $\arg[\sqrt{\mu+\lambda_{\rm h}}] \in (0,\frac{1}{2}\pi)$ (see (5.14)) and $\arg[1/\sqrt{\mu+\lambda_{\rm h}}] \in (-\frac{1}{2}\pi,0)$. Hence, $\mathrm{Re}[1/\sqrt{\mu+\lambda_{\rm h}}] > 0$, so that

$$\mathrm{Re}[\mathcal{G}_2(\ell_{\rm vert},\mu)\gamma_{\rm r}^2]|_{\gamma_{\rm r}=\pm 1} > \mathrm{Re}[\mathcal{G}_2(\ell_{\rm vert},\mu)\gamma_{\rm r}^2]|_{\gamma_{\rm r}=0} = 0,$$

which implies that the parabolic belly of $\Lambda_{\rm h}(\ell_{\rm vert},\mu)$ points to the left, that is, away from the imaginary axis if $\Lambda_{\rm h}(\ell_{\rm vert},\mu)$ is contained in the stable complex half plane. Therefore, it is impossible for interior points of $\Lambda_{\rm h}(\ell,\mu_{\rm dest})$ to cross through the imaginary axis before the endpoints $\partial_\pm\Lambda_{\rm h}(\ell,\mu_{\rm dest})$ do. Since $\Lambda_{\rm h}(\ell,\mu)$ rotates as function of ℓ, there must be values of $\mu_{\rm dest}(\ell)$ for which both endpoints $\partial_\pm\Lambda_{\rm h}(\ell,\mu_{\rm dest})$ are on the imaginary axis. Such situations correspond to the co-dimension 2 bifurcation at which $\mathcal{H}_{+1}$ and $\mathcal{H}_{-1}$ intersect.

Finally, we note that the higher order, non-quadratic, corrections to the shape of $\Lambda_{\rm h}(\ell,\mu_{\rm dest})$ – see Lemma 5.6 – cannot have an effect on the above considerations. □

The fact that the parabolic belly always points away from the imaginary axis indeed is quite intriguing. In Figure 4.9, a sketch is given of the combined Hopf and belly dance: the belly 'dances' with twice the frequency of the rotation of the spectral

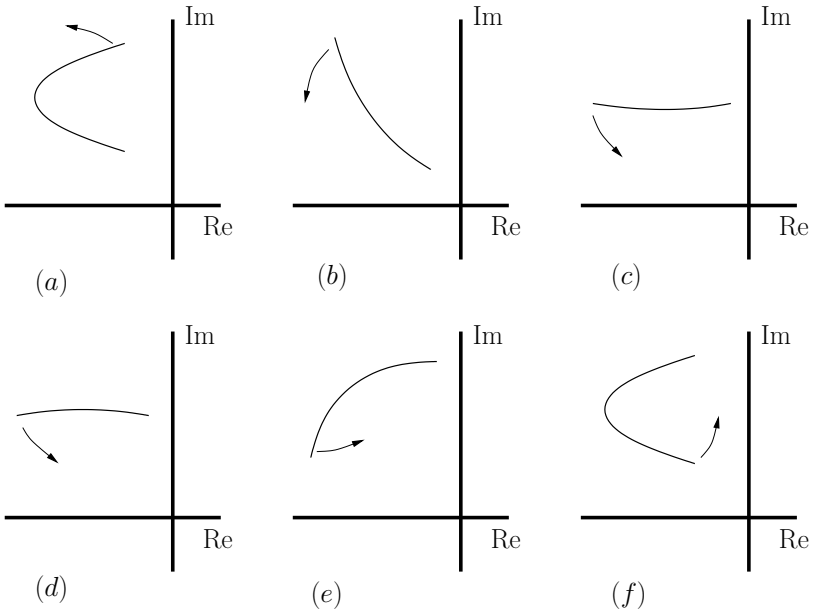

Figure 4.9: A sketch of the combined Hopf and belly dances of the spectral curve Λ_{h} for values of μ and k inside the Busse balloon. Wavenumber k decreases in a series of snapshots from (a) to (f), the picture shows a series of snapshots of Λ_{h}. The arrow indicate the direction of the rotation. Notice that this sketch does not include the exponential decay of the scale of the curve as k decreases and that (the higher order effect of) its bending has been exaggerated. Compare to Figure 4.6.

curve. The belly dances causes the boundary of the Busse balloon to be as sketched in Figure 4.10(a). Although we have just shown that this does not occur in equations of the type (1.2)/(1.4), it would a priori have been natural to expect that also the situation as presented in Fig 4.10(b) could occur. Here the boundary of a Busse balloon is sketched in the hypothetical situation that parabolic belly is oriented towards the imaginary axis near the bifurcation: ($\mathcal{O}(1)$) close to the intersections of $\mathcal{H}_{+1}$ and $\mathcal{H}_{-1}$ there is a small region in which the pattern $(U_{\mathrm{p}}(\xi;L), V_{\mathrm{p}}(\xi;L))$ is destabilized by an 'internal Hopf bifurcation' at $\gamma_{\mathrm{r}}^{\mathrm{int}} \neq \pm 1$. In the final section we discuss whether this scenario indeed is impossible (especially in the light of Remark 1.4).

4.6 Discussion

In this chapter we have found, by numerical means, that the Busse balloon associated to periodic patterns in the Gray-Scott model (with $\varepsilon^4 = 0.001$ and $B = 0.026$) has a fine structure consisting of a Hopf dance of snaking bifurcation curves $\mathcal{H}_{\pm 1}$ with many co-dimension 2 intersections. This phenomenon has been established as a

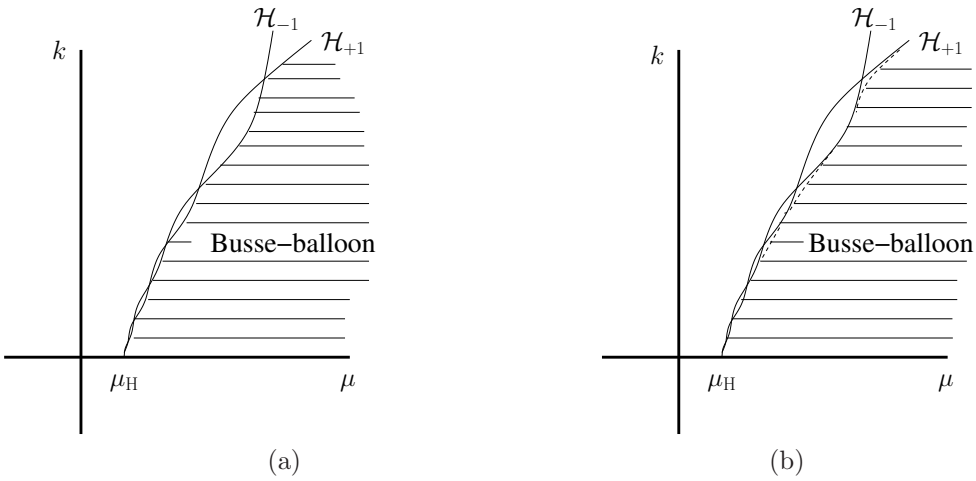

Figure 4.10: A typical sketch of the snaking curves $\mathcal{H}_{+1}$ and $\mathcal{H}_{-1}$.(a) The situation as established by the analysis: the belly of Λ_{h} always points into the stable half plane near the intersections of $\mathcal{H}_{\pm}$ (b) The hypothetical scenario in which the belly would be oriented towards the unstable half plane: there are no co-dimension 2 bifurcations near the homoclinic tip, but the intersection of $\mathcal{H}_{\pm 1}$ are preceeded by 'interior' Hopf bifurcations as the spectral branch Λ_{h} crosses the imaginary axis for some γ-eigenvalue with $\gamma \notin \{\pm 1\}$.

generic destabilization mechanism by a detailed analysis of the destabilization of long wavelength, nearly localized, stationary, reversible spatially periodic patterns in the class of two component, singularly perturbed reaction-diffusion systems represented by the normal form model (1.4).

The main open question of course is: *'Does the Hopf dance destabilization mechanism persist beyond the range of singularly perturbed two component reaction-diffusion systems?'* We strongly believe that this is the case. Since the destabilization mechanism concerns the behavior of nearly homoclinic patterns, it is expected that it is possible to establish the validity of the Hopf dance mechanism for non-singularly perturbed N-component reaction-diffusion equations by extending the methods developed in [36, 78]. We do have to be a careful, though. A first look into the applicability of the methods of [36, 78] to this problem suggests that it is possible to establish the persistence of the stretching and rotating behavior of the (collapsed) spectral curves near the homoclinic limit. By the general theory presented in section §4.2, this would imply that the Hopf dance mechanism indeed also appears as a generic feature is this much larger class of systems.

However, at this point it is not at all clear whether or not the belly dance also persists, and more importantly: in what way it persists. We expect that the boundary of the

Busse balloon near the homoclinic limit does not necessarily have to be of the type sketched in Figure 4.10 (a), i.e. the structure associated to the Gray-Scott system and to the normal form. This feature may be related to the character of the models (1.1) and (1.4). It follows from a detailed re-examination of the proof of Corollary 5.7 that the orientation of the belly is in essence determined by the exponential terms $E(\lambda, \ell)$ in the expression for the Evans function given in Theorem 4.2. In general, we do not expect such exponential terms in the Evans function associated to the stability of stationary patterns. In fact, it is for this reason to be expected that the belly dance may already change orientation in the class of singularly perturbed two component models presented in Remark 1.4: the results to be presented in [13] seem to imply that the role of the exponential expressions $E(\lambda, \ell)$ may be taken over by more general expressions. These expressions may cause the orientation of the belly in the Hopf dance to change. Note that this (so far quite formal) observation does not 'destroy' the generiticity of the Hopf dance, it only shows that the orientation of the belly dance may change if one considers a larger class of models. In fact, it shows that the two Hopf dance scenarios shown in Figure 4.10 may both occur (and thus not only the one given in Figure 4.10(a)). Of course, this all is at present not yet established as a rigorous mathematical result: it is the subject of work in progress.